Cy. 2
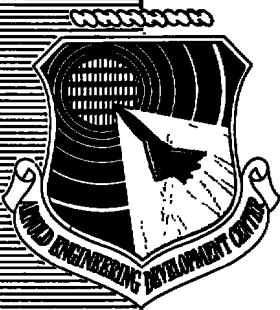
AFML CERAMIC NOSETIP ABLATION TEST

PROPULSION WIND TUNNEL FACILITY
ARNOLD ENGINEERING DEVELOPMENT CENTER
AIR FORCE SYSTEMS COMMAND
ARNOLD AIR FORCE STATION, TENNESSEE 37389

December 1975

Final Report for Period February — April 1975

Approved for public release; distribution unlimited.

Prepared for

AIR FORCE MATERIALS LABORATORY (MXS)
WRIGHT-PATTERSON AFB, OHIO 45433

This report has been reviewed by the Information Office (OI) and is releasable to the National Technical Information Service (NTIS). At NTIS, it will be available to the general public, including foreign nations.

APPROVAL STATEMENT

This technical report has been reviewed and is approved for publication.

FOR THE COMMANDER

JOHN C. CARDOSI
Lt Colonel, USAF
Chief Air Force Test Director. PWT
Directorate of Test

CRAIG E. MAHAFFY
Colonel, USAF
Director of Test

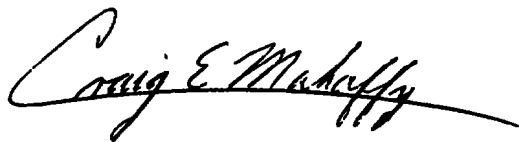| REPORT DOCUMENTATION PAGE		READ INSTRUCTIONS BEFORE COMPLETING FORM
1 REPORT NUMBER AEDC-TR-75-115	2 GOVT ACCESSION NO.	3 RECIPIENT'S CATALOG NUMBER
4. TITLE (and Subtitle) AFML CERAMIC NOSETIP ABLATION TEST		5. TYPE OF REPORT & PERIOD COVERED Final Report - February - April 1975
		6. PERFORMING ORG. REPORT NUMBER
7 AUTHOR(s) J. B. Patton and H. F. Lewis - ARO, Inc.		8. CONTRACT OR GRANT NUMBER(s)
9 PERFORMING ORGANIZATION NAME AND ADDRESS Arnold Engineering Development Center (XO) Arnold Air Force Station Tennessee 37389		10. PROGRAM ELEMENT, PROJECT, TASK AREA & WORK UNIT NUMBERS Program Element 62102F Project 7381
11. CONTROLLING OFFICE NAME AND ADDRESS Air Force Materials Laboratory (MXS) Wright-Patterson AFB, Ohio 45433		12. REPORT DATE December 1975
		13. NUMBER OF PAGES 64
14 MONITORING AGENCY NAME & ADDRESS(if different from Controlling Office)		15. SECURITY CLASS. (of this report) UNCLASSIFIED
		15a. DECLASSIFICATION/DOWNGRADING SCHEDULE N/A

16 DISTRIBUTION STATEMENT (of this Report)

Approved for public release; distribution unlimited.

17 DISTRIBUTION STATEMENT (of the abstract entered in Block 20, if different from Report)

18. SUPPLEMENTARY NOTES

Available in DDC

19 KEY WORDS (Continue on reverse side if necessary and identify by block number)

AFML Ceramic Nose Tip
ablation
test methods
test facilities (free-jet)

arc heaters
air
high temperature
Mach numbers

20 ABSTRACT (Continue on reverse side if necessary and identify by block number)

Eight ablation test runs were made in an arc-heated, free-jet facility using air as the test fluid. These tests were made to study the effects of hyperthermal conditions on ablative materials of various compositions. The study was accomplished at Mach numbers 2.0 and 2.3 with measured reservoir pressures ranging from 78.2 to 142.2 atm and total bulk enthalpies from 2,120 to 2,416 Btu/lb. For the above conditions, model stagnation pressures

DD $_{1 \text{ JAN } 73}^{\text{ FORM}}$ 1473   EDITION OF 1 NOV 65 IS OBSOLETE

UNCLASSIFIED

20. ABSTRACT (Continued)

ranged from 42.9 to 92.8 atm. The models consisted of sphere-
cone and cone-cone configurations. A pressure probe was used to
obtain model stagnation pressure, and a multichannel calorimeter
model was used to obtain heat-transfer data for flow calibration.

AFEC
Arnold AFB Tenn

UNCLASSIFIED

PREFACE

CONTENTS

TABLES

1.0 INTRODUCTION

The primary objective of the AFML-Avco System ablation program was to investigate the ablation characteristics of ceramic materials with different microscopic structures under conditions of high pressure and temperature. The accomplishment of the objective was supported by ablation testing in the Arc Heater Test Unit (5-MW) of the Propulsion Wind Tunnel Facility (PWT) at the Arnold Engineering Development Center (AEDC).

The models tested are referred to in this report by coded designation only. The fabrication technique, reinforcing methods, and material composition of the models are not listed. For information concerning model material, contact AFML/MXS, Wright-Patterson Air Force Base, Ohio.

This report presents a description of the test facility, instrumentation, model configuration, operational procedure of the test program, and documented test results with a minimum analysis of the data.

2.0 DESCRIPTION OF TEST FACILITY

2.1 GENERAL

The (5-MW) Arc Heater is a continuous flow, arc-heated tunnel using air and is equipped for tests of ablation materials over a wide range of reentry conditions.

The test unit consists of the arc heater, nozzle assembly, rotary model injection system, laser-controlled model advance system, and auxiliary systems of high-pressure air, high-voltage d-c power, demineralized water, raw water, exhausters, and instrumentation. A photograph of the test unit is shown in Fig. 1.

2.2 ARC HEATER

The test unit is driven by a modified version of a Linde® Model N4000 arc heater, nominally rated at 5 MW, which is shown schematically in Fig. 2 and described in Refs. 1 and 2.

During operation, the arc is maintained between tandem electrodes which are separated by a chamber in which air is injected tangentially. The resulting radial pressure gradient tends to stabilize the primary arc column. A highly complex energy exchange raises the energy level (enthalpy and pressure) of the gas prior to expansion through the nozzle downstream of the front electrode.

2.3 NOZZLE CONFIGURATIONS

The ·nozzles available for use in the facility are listed in Table 1, including the dimensions and maximum model impact pressures produced with each. Two conventional expansion nozzles, Mach numbers 2.0 and 2.3, and one type of shrouded flow nozzle were used during the test. In general, conventional nozzles are used for testing at high impact pressures, and the shrouded nozzle is used for tests which require large model sizes at lower pressures.

Conventional flow nozzles are available for achieving various stagnation conditions on test models. The nozzles are water cooled and are designed to provide a uniform flow field at the nozzle·exit. A schematic of a typical conventional nozzle is shown in Fig. 3.

By surrounding the arc-heated flow with a coaxial shroud of high-pressure cold air, the effective diameter of the test jet is increased. The pressure simulation over the model is established mainly by the large annular cold-flow jet, while the hot core supplies the annular region near the model with high energy gas. The total flow diameter provided by the shrouded nozzle is 1.213 in. In the internal cold shroud nozzle (ICS), Fig. 4, the shroud air is introduced inside the nozzle upstream of the sonic point. The ICS configuration minimizes the bow shock interface disturbances in the exit flow.

2.4 ROTARY MODEL INJECTION SYSTEM

The test unit is equipped with a multiple-arm, seven-position, remotely controlled rotary model injection system (Fig. 5). Models can be positioned sequentially on the test stream centerline for preset dwell times ranging from 1.0 sec to 1.0 min. The arc heater conditions remain essentially constant during a test run. Nearly constant injection velocity is provided during the index cycle between normal stop positions and, by using 45-deg offset arms between positions, transient calibration probes can be swept through the test stream. In this configuration, sweep speeds ranging from approximately 20 to 60 in./sec can be attained.

The model injection system can be operated with the carriage in a fixed position and with the support arms rotating in a fixed plane, in which case, the axial position of each model with respect to the nozzle exit is set by means of a frictional clamp between the model sting and the support arm. Model-mounting interface and maximum outline dimensions are shown in Fig. 6.

2.5 LASER-CONTROLLED MODEL ADVANCE SYSTEM

The axial extent of the uniform pressure region downstream of the nozzle is a function of the exit diameter and Mach number. The ablating surface of a model frequently moves completely out of the uniform flow region. To counter this recession and to keep the ablating surface in the region of uniform flow, the entire model injection system is driven axially with a hydraulic system. The drive rate is essentially the same rate at which the model ablates, thus holding the model front surface in the uniform flow field.

A schematic of the model advance system in relation to the test unit and a block diagram of the laser control system are presented in Fig. 7. The model advance system incorporates a laser beam propagated through the centerline of the plasma stream and detected by a photocell sensor. While the laser beam is blocked by the model front surface to a preset beam percentage null point, a command signal is sent to the servovalve and hydraulic cylinder to stop forward movement. When the model recedes approximately 0.002 in. and the laser beam is partially uncovered, the photocell signals the axial drive system to move forward to the null point. The model front surface is thereby kept at virtually a fixed position with respect to a predetermined test station.

2.6 AUXILIARY SYSTEMS

Air for the arc heater is supplied directly from compressors, and air for the shrouded nozzle is supplied from storage bottles, both at 4,000-psi maximum pressure. Controls and metering stations complete the system. High-voltage d-c power is supplied through a system of a-c transformers and a 10-MW, three-phase, full-wave ignitron rectifier. Demineralized water to cool the arc heater is supplied by two high-pressure (650 psig) pumps, and raw water for cooling the nozzle is supplied from a single pump at pressures up to 1,000 psig. The exhaust system consists of an inlet section, a short section of water-jacketed ducting, a section of uncooled ducting, and a vertical duct with a single stage, axial-flow fan discharging to atmosphere.

3.0 INSTRUMENTATION

3.1 TEST UNIT INSTRUMENTATION

Test unit instrumentation consists of visual indicators and recording equipment. Visual observation of pressures during a run is accomplished by use of Autosyn® transmitters and indicators. Test unit temperatures are measured by various types of thermocouples and pulse rate converters. Arc voltage and current are measured by use of a voltage divider and a current shunt. All data necessary to calculate arc heater performance are recorded on either a strip chart recorder or a high-speed oscillograph.

3.2 FLOW CALIBRATION INSTRUMENTATION

Flow calibration in the 5-MW Arc Heater was monitored on each run by use of transient diagnostics probes which were swept across the flow in a time period of approximately 30 msec. Impact pressure profiles were measured with a multichannel probe having a nose radius of 0.25 in. and an orifice diameter of 0.048 in. (Fig. 8a). The pressure transducers were internally mounted, piezoelectric types. The outputs were measured by charge amplifiers, further amplified by precision d-c amplifiers, and eventually recorded on a high-speed oscillograph having paper speeds up to 160 in./sec. Total volume of the capillary sensing tube and transducer chamber is such that response times of 1 msec are typical.

The stagnation point heat-transfer profile of the flow was measured with a transient calorimeter probe, Fig. 8b, in which the thermocouple junction was located at the "null-point", i.e., that critical depth below the gage surface at which the temperature response is the same as that which would occur at the model surface if there were no thermocouple cavity. Data from these gages were reduced by a one-dimensional heat conduction computer program which used, as input, the surface temperature variation inferred from the null-point calorimeter.

The axial variation of impact pressure downstream of the nozzle exit (from approximately 0.1 to 4.0 in.) was measured during Runs 4 and 4A by use of a pressure probe having a slow traverse. The relatively long immersion time of this probe required that it be fabricated from graphite (Fig. 9).

3.3 ABLATION MODEL INSTRUMENTATION

The surface brightness temperatures of the ablating models were measured by miniature pyrometers. Filters were utilized with the pyrometers to extend their range to upper limits of approximately 7,000°R.

Three high-speed, motion-picture cameras were provided to record ablating surface changes during exposure to the jet stream. Operating speeds up to 600 frames/sec were available. Camera locations, lens settings, type of filters, and operating speeds were set depending on the run requirements. Camera type, film type, lens and camera setting, and filters used during each run are listed in Table 2.

4.0 DESCRIPTION OF TEST MODELS

The test models and holders were furnished by Avco Systems. Two model configurations were used, one a sphere-cone (S) with 0.25-in. nose radius (R_n) and 7-deg

cone half-angle (θ), the other a cone-cone (C) with a 0.075-in. nose radius (R_n) and cone half-angles (θ_1, θ_2) of 50 and 7 deg, respectively. A sketch showing the model configurations, dimensions, and assembly is presented in Fig. 10. The fabrication technique and material composition of the models were not known; however, Avco Systems Division identified the models through a coding system. Figure 11 is a photograph of model and holder.

The test conditions, model configuration, and calibration probes for each test run are presented in Table 3.

5.0 TEST PROCEDURE

5.1 MODEL PREPARATION

The test models were photographed, Fig. 12, weighed, and measured prior to being mounted in the holders. The model assemblies were mounted to preselected stings, Fig. 6, and were centered in the nozzle exit flow with nosetips at a fixed distance (X) from the nozzle exit plane (Typical X = 0.10 in.). The two calibration probes (calorimeter and pressure, Figs. 8a and b) were mounted on offset arms, aligned, and set at the desired distance (X) from nozzle exit (see Table 3). The offset arms allow the calibration probes to be swept through the flow with little or no damage. Use of this mode of operation allowed the probes to be reused on subsequent test runs.

5.2 TYPICAL RUN

Prerun electrical calibrations of the arc heater test unit instrumentation and model instrumentation were made. The sequence of events during a test run was (1) energize the arc heater and (2) establish the test conditions, allowing approximately 20 sec for the cooling water temperature to stabilize. At this time, the model data recording equipment and motion-picture cameras were started. The models were then injected. After all models had been cycled through the flow, the test unit was de-energized, and a postrun electrical calibration of the instrumentation was performed.

6.0 DATA PRECISION

6.1 MEASURED VALUES

The measured model weights are estimated to be correct within ±1.0 mg, and the length measurements are estimated to be within ±0.001 in. The measured values of pressure are estimated to be correct within ±1 percent.

6.2 CALCULATED VALUES

Tunnel reservoir total enthalpy is calculated by energy conservation considerations and is subject to an uncertainty of ±10 percent. This uncertainty was calculated using the precision values for the various measuring devices involved and assuming error propagation by use of a Taylor's series.

Values of heat-transfer rate calculated from the temperature response of a null-point calorimeter are subject to an uncertainty which is very difficult to quantify. There is, at present, no accurate and reliable way to calibrate these devices for the high heat-transfer rates associated with arc-heated facilities. An indication of the accuracy, however, can be obtained from the fact that the measured heating rates approach within ±5 percent of laminar Fay-Riddell values when the heater is operated with a stilling chamber upstream of the nozzle. Also, the digital computer code used for heat-transfer data reduction at AEDC agrees within ±5 percent with two other codes when supplied with the same inputs. A conservative estimate would be that the total uncertainty in heat-transfer-rate values is ±15 percent.

7.0 RESULTS AND DISCUSSION

7.1 PRESSURE MEASUREMENTS

Pressure measurements of two kinds were made during the test period: radial sweeps with the nosetip of the probe shown in Fig. 8a positioned at various axial locations, and axial traverses with the orifice of the probe shown in Fig. 9 located on the nozzle centerline approximately 4 in. downstream from the nozzle exit and then driven upstream toward the exit of the nozzle.

7.2 RADIAL PRESSURE PROFILES

The results of a radial sweep made 0.1 in. downstream from the exit of the conventional Mach number 2.0 nozzle are shown in Fig. 13. For the radial sweeps, the probe was mounted on an offset arm (see Fig. 5) with the tangential velocity nominally about 25 in./sec. Since the gas velocity at the nozzle exit ranged from about 7,000 to 8,000 ft/sec, the angle of attack induced by the relative motion of probe and gas was infinitesimal, and had no effect on the pressure measurements. There were little or no unsteady flow effects since the characteristic time for a small slug of gas to traverse the length of the probe is very small compared to the sweep characteristic time. The profiles, however, would be affected by the probe size and the degree of underexpansion at the nozzle exit. Taking these things into consideration, the radial pressure uniformity is quite good for the conventional nozzles, Mach numbers 2.0 and 2.3, respectively (Figs. 13 and 14).

Radial pressure ratio profiles obtained from the Mach number 2.0 ICS nozzle are shown in Fig. 15. The same comments apply as for the conventional nozzle profiles, except that additional effects occur because of mixing and differences in total pressure, Mach number, and specific heat ratio between the hot and cold coaxial jets.

7.3 SPHERE-CONE PRESSURE DISTRIBUTIONS OBTAINED DURING RADIAL SWEEP

Figure 16a presents the results of sphere-cone pressure measurements made during radial sweeps with a conventional Mach number 2.0 nozzle and the multichannel pressure probe shown in Fig. 8a. These are values read when the pressure probe was on the jet centerline. Two reference curves are shown, for Mach numbers 2.50 and 10.0, calculated for $\gamma = 1.2$ by the inviscid theory of Ref. 3. Near the nozzle exit at 30 deg on the spherical nose the data and theory agree. Near and downstream from the model shoulder, however, the data fall below the theoretical values. This is because of the small-diameter jet stream (0.51 in.) and underexpansion at the nozzle exit. Figure 16b shows the comparison between theory and data for the Mach number 2.3 nozzle, and the same comments apply as for the Mach 2.0 nozzle.

The comparisons for the Mach number 2.0 ICS nozzle are shown in Fig. 17, and the agrement is much improved. This is because the jet diameter is about 1.2 in. at the exit as contrasted with 0.51 in. for the conventional nozzle, and therefore, the pressure distribution is nearer the flight case. The cold shroud nozzle, therefore, improves the pressure distribution simulation and also saves on electrical energy. A history of the development of the shrouded nozzle test concept is given in Ref. 4.

7.4 AXIAL PRESSURE TRAVERSES

One of the test requirements was to position ablation models initially at a location downstream from the nozzle exit where the impact pressure was about 5 atm and then to move the model toward the nozzle at a rate of speed so as to approximate the flight reentry pressure history. Figure 18 presents typical reentry pressure histories for entry angles of -20 and -40 deg and the results of two axial traverses from Runs 4 and 4A with the Mach number 2.0 ICS nozzle. By varying the nozzle reservoir pressure and the probe traverse speed, the pressure history required for a given trajectory can be closely approximated, and this technique was used during test Runs 5, 6, and 7.

7.5 HEAT-TRANSFER-RATE MEASUREMENTS

Radial sweeps of a sphere-cone probe (Fig. 8b) instrumented with null-point calorimeters were made to obtain heat-transfer-rate measurements.

Null-point calorimeters (see Ref. 5) are devices designed to simulate the temperature response of a one-dimensional, semi-infinite slab which is accomplished by the proper location of a subsurface thermocouple in a cylindrical metal slug of the proper geometry. The calculation of heat-transfer rate to such a slug is well developed, and in this case, this temperature history and slug thermophysical properties are used in a digital computer program based on the method of Ref. 6. The probe is swept across the flow at a speed sufficient to prevent overheating, or melting, of the calorimeter slug. For the pressure and enthalpy levels prevailing during this test program, a sweep time of about 30 msec was adequate.

Some typical heat-transfer profiles obtained by sweeping the calorimeter probe across the flow are presented in Figs. 19a through f. Both the measured hot wall heat flux and the corresponding cold wall heat flux profiles are presented. It is noted that, because of arc heater fluctuations, the short-term average heat flux value obtained from a single 30-msec sweep will be different than the long-term average value obtained from a large number of sweeps, representing approximately a period of 2 to 4 sec. The long-term average heat flux value, shown in Fig. 19, has been found to be very close to 1.7 times the laminar Fay-Riddell heat flux value, based on large quantities of data generated in the AEDC 5-MW Arc Heater (Ref. 7). Figure 20 shows hot wall heat-transfer rate as a function of the Fay-Riddell parameter, $H_o\sqrt{p_o'/R_n}$ $(1 - h_w/H_o)$, for sixteen traverses (five from this test). The data spread is from minimum to maximum values over a 0.5-in. core of the flow, with the symbol representing the average over the core. These data lie within a typical scatter band about the 1.7 times Fay-Riddell long-term average scatter value. Free-stream turbulence is believed to be the reason for the factor of 1.7; it is known that the interposing of a mixing or stilling chamber between the arc heater and the test nozzle results in heat-transfer rates nearly equal to those predicted by the Fay-Riddell theory.

7.6 ABLATION DATA

Four series of ceramic models, designated A-1, A-2, A-3, and A-4 were tested. Graphite models were also tested, and the results were used for comparison with ceramic model ablation data. The ablation rate data were recorded on film using high-speed cameras. This film was transmitted to Avco for analysis. The maximum model brightness temperatures as recorded are presented in Table 4. Model pretest and posttest weights and lengths are listed in Table 3. The posttest photographs presented in Figs. 21a through g provide a basis to make a preliminary relative ranking of the materials tested within a run or runs at similar environmental conditions. In Figs. 21c and g, it is seen that the "A" series ceramic models ablate faster than graphite models 8S-12-1 and -2. A complete evaluation of the materials and an extensive study of each series of models tested are being conducted by the Avco Systems Division.

REFERENCES

1. Henson, J. R. "Ablation Tests of Sphere-Cone Models in the AEDC 5-MW Facility." AEDC-TR-70-194 (AD873345), August 1970.

2. Henson, J. R. "AFML Materials Ablation Tests in the AEDC 5-MW Facility, Series II." AEDC-TR-71-11 (AD879312), January 1971.

3. Weilerstein, Gertrude. "The Addition of Secondary Shock Capability and Modifications to the GASL Three-Dimensional Characteristics Program, Part II. User's and Programmer's Manual." GASL-TR-653 (AD666742), August 1967.

4. Smith, R. T. and Pigott, J. C. "Further Evaluation of a New Facility Concept for Testing Large Ablation Models at High Stagnation Pressures." AEDC-TR-71-212 (AD731142), October 1971.

5. Kennedy, W. S., et al. "Heat Flux Measurement using Swept Null Point Calorimetry." AIAA Paper No. 71-428, April 1971.

6. Cook, W. J. and Felderman, E. J. "Reduction of Data from Thin-Film Heat-Transfer Gages: A Concise Numerical Technique." AIAA Journal, March 1966, pp. 561-562.

7. Smith, R. T., MacDermott, W. N., and Giltinan, T. L. "A Transient Enthalpy Probe for the Calibration of High Heat Flux Ablation Facilities." AEDC-TR-74-116 (ADA003950), January 1975.
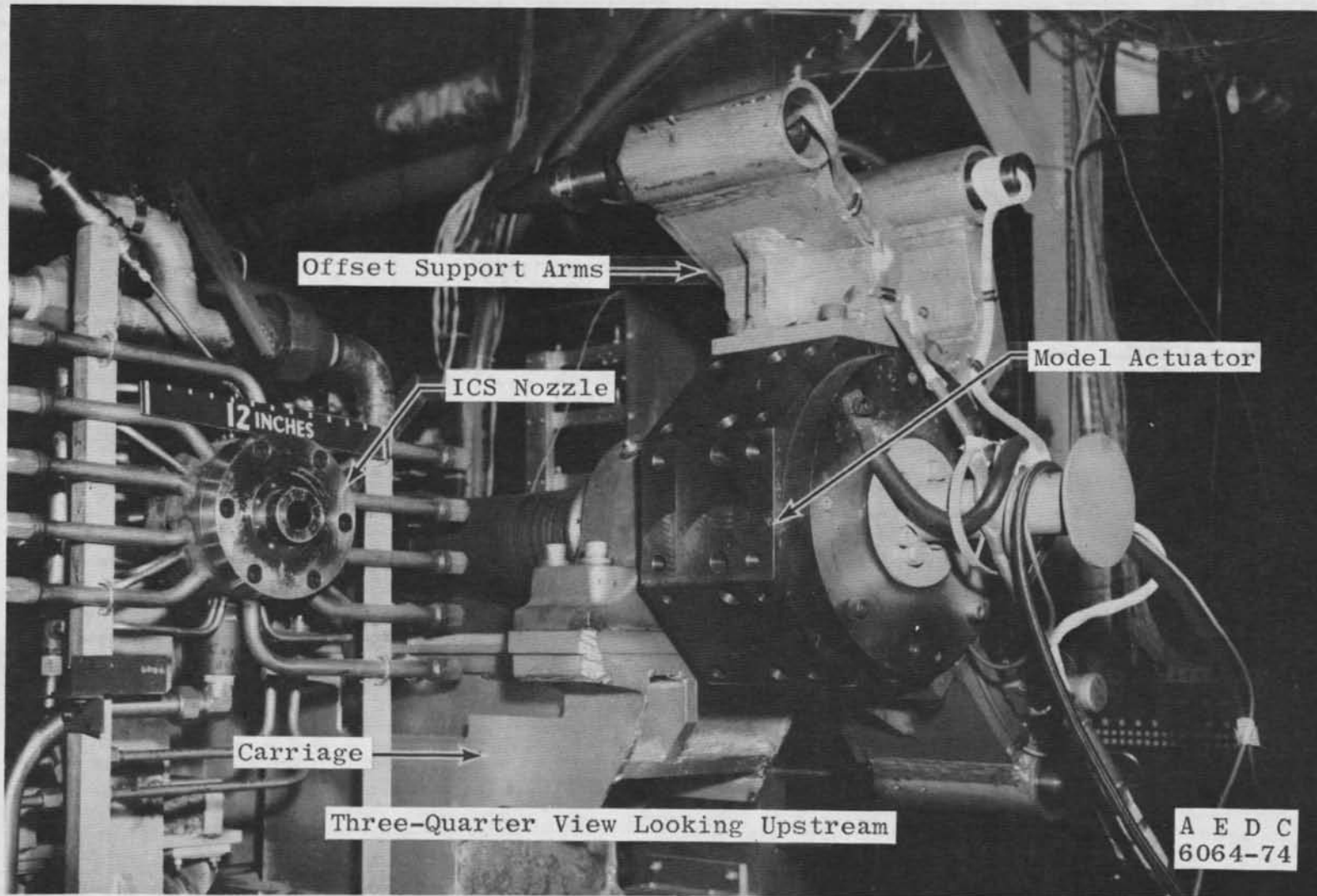
Figure 1. Arc Heater Test Unit (5MW).
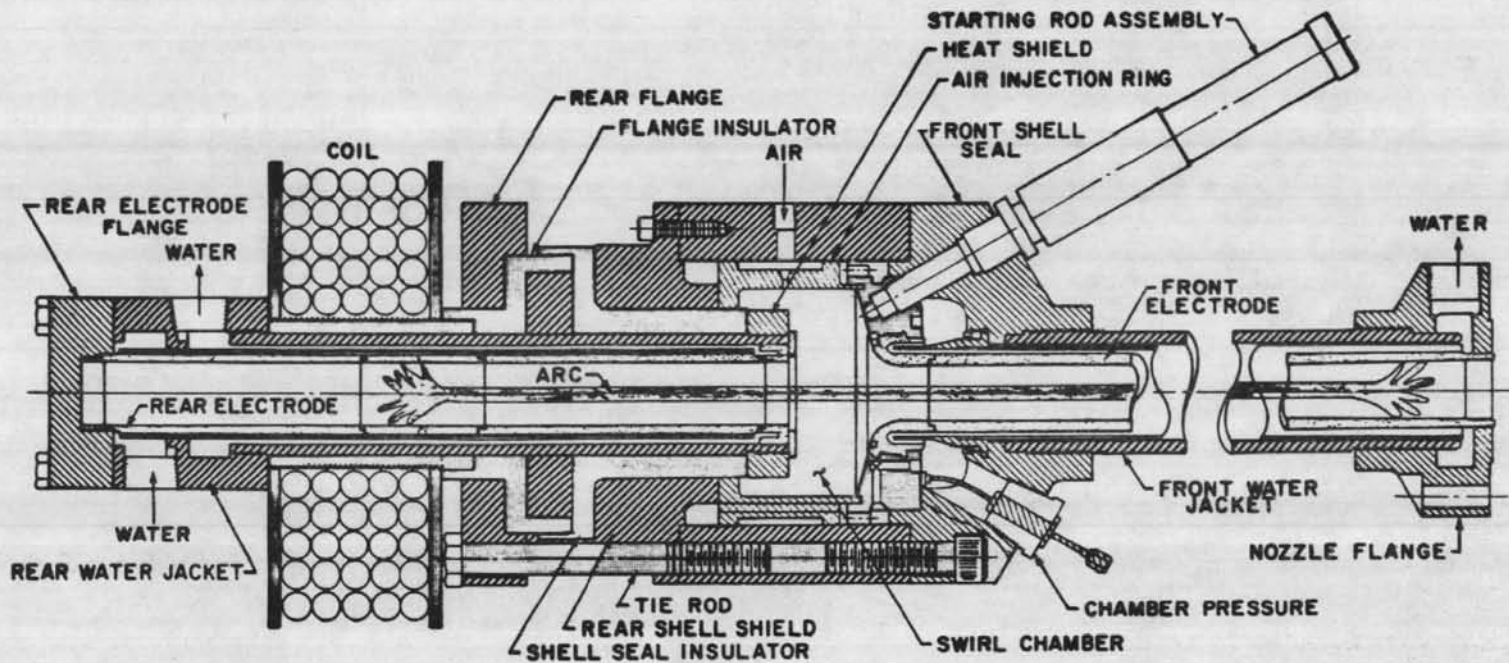
Figure 2. Arc heater schematic.

Water Water

NOZZLE
HOUSING

NOZZLE
LINER

0.518

FLOW

MACH NO. 2.0
$d^* = 0.375$

WATER
BLOCKS

ARC HEATER
NOZZLE FLANGE

ALL DIMENSIONS IN INCHES
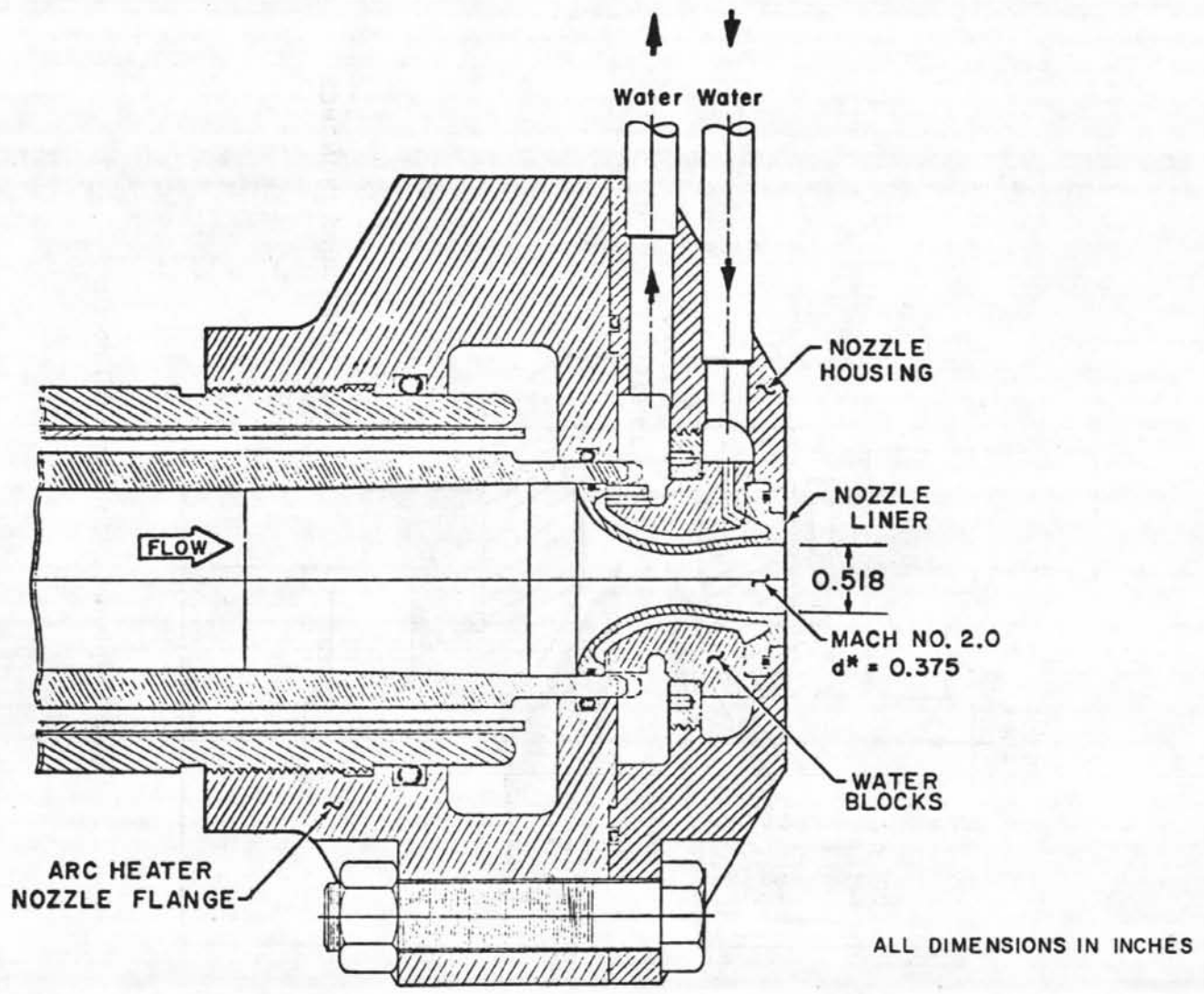
Figure 3. Conventional nozzle schematic.

COLD
SHROUD
AIR

COOLING
WATER

ARC-HEATED
AIR →

0.372 D

1.2134 D

0.9188 D

ALL DIMENSIONS IN INCHES
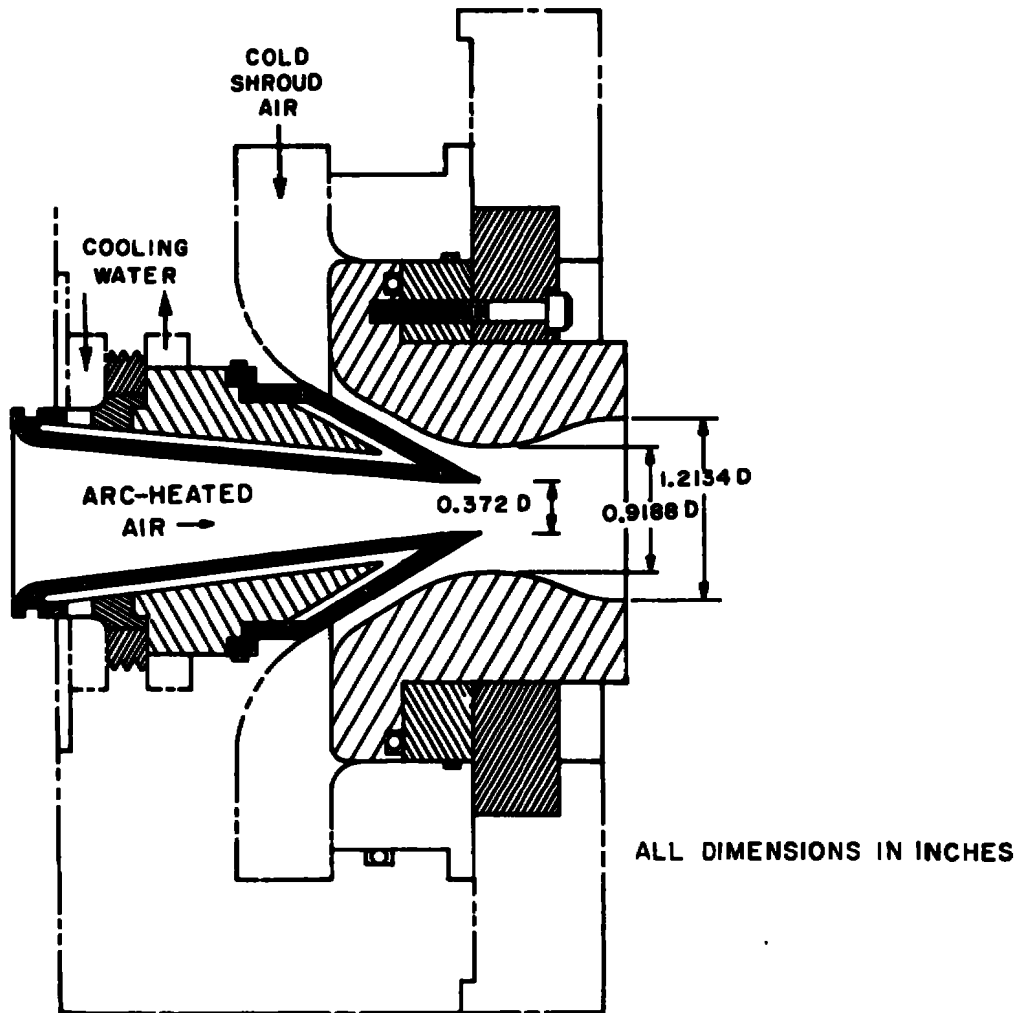
Figure 4. Internal cold shroud (ICS) nozzle.
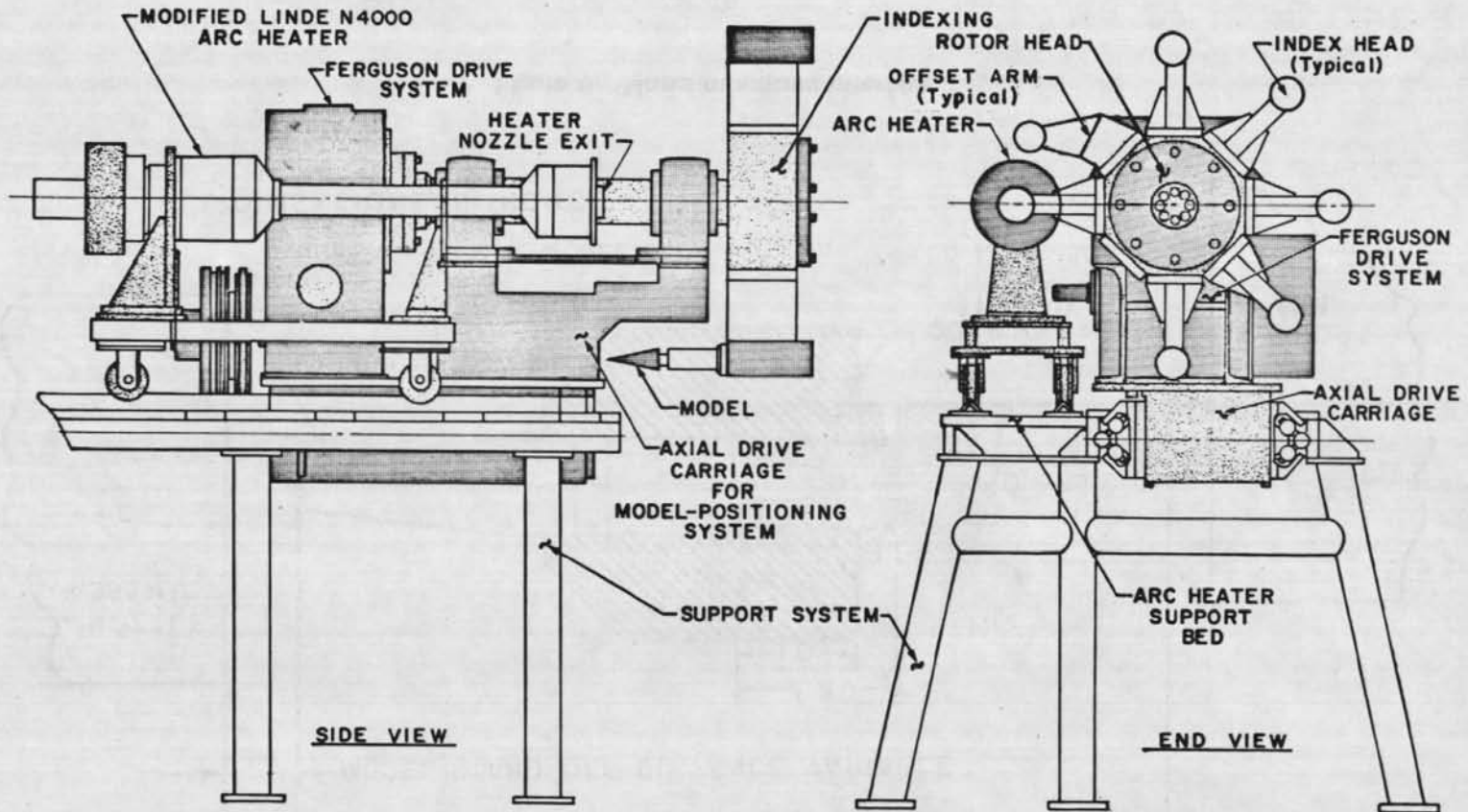
Figure 5. Rotary model injection system.

MODIFIED LINDE N4000
ARC HEATER

FERGUSON DRIVE
SYSTEM

HEATER
NOZZLE EXIT

INDEXING
ROTOR HEAD

OFFSET ARM
(Typical)

ARC HEATER

INDEX HEAD
(Typical)

FERGUSON
DRIVE
SYSTEM

AXIAL DRIVE
CARRIAGE

MODEL

AXIAL DRIVE
CARRIAGE
FOR
MODEL-POSITIONING
SYSTEM

SUPPORT SYSTEM

ARC HEATER
SUPPORT
BED

SIDE VIEW

END VIEW
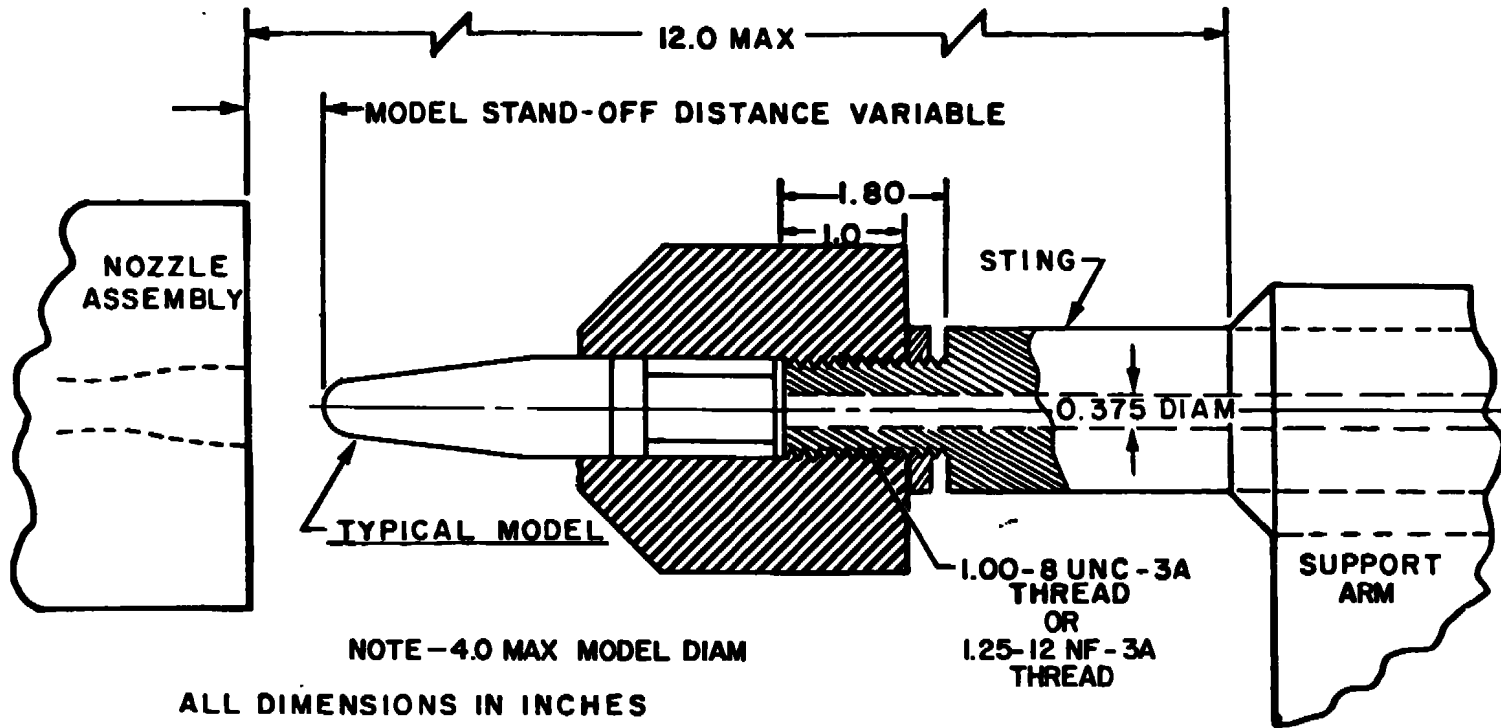
Figure 6. Model-mounting interface.
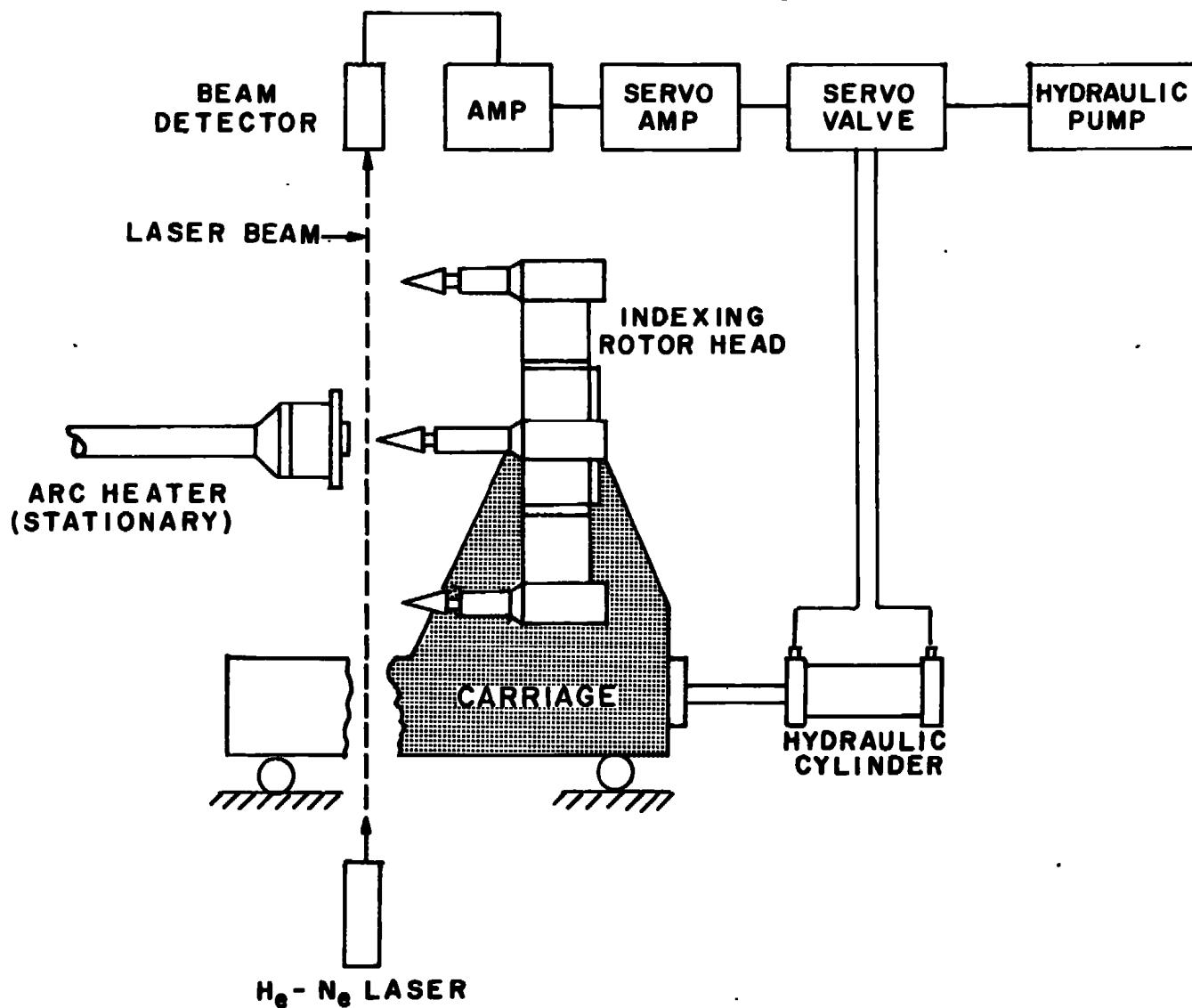
Figure 7. Laser-controlled model advance system.
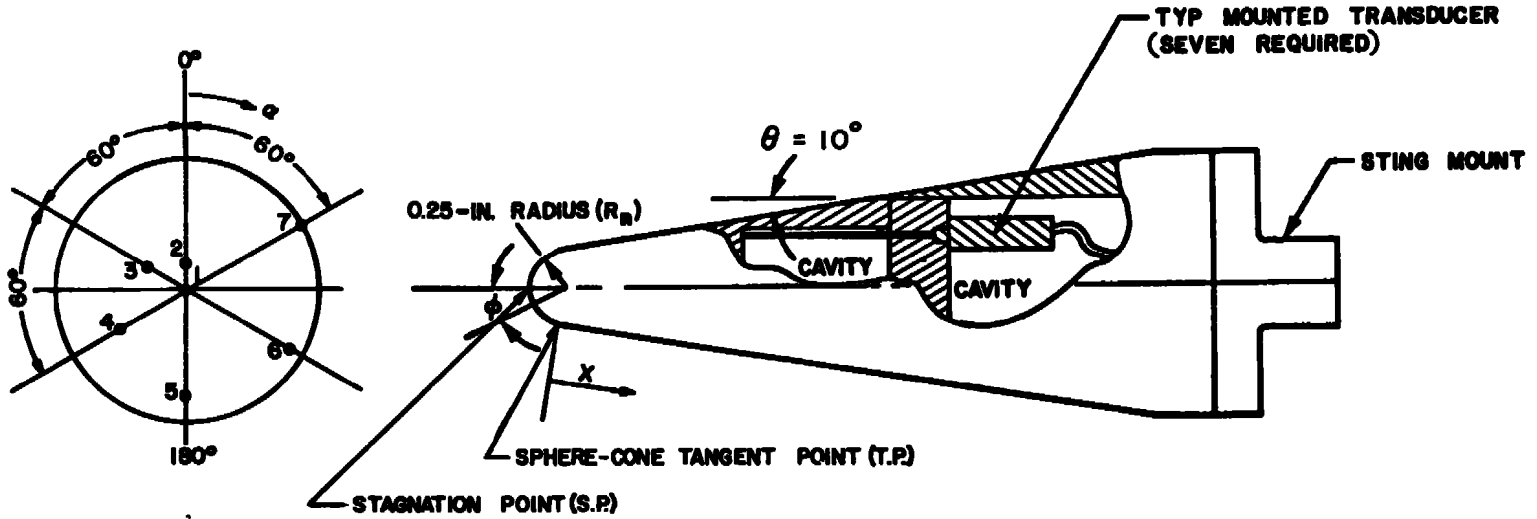
Pressure Tap	S/R_n	ϕ, deg	α, deg	X, in.
1	0	S.P.	S.P.	S.P.
2	0.524	30	0	N.A.
3	1.310	75	300	N.A.
4	2.100	80*	240	0.175*
5	2.600	80*	180	0.300*
6	3.800	80*	120	0.600*
7	4.400	80*	60	0.750*

*Pressure tap located X distance
downstream of tangent point.

NOTE: NOT TO SCALE

a. Pressure
Figure 8. Multichannel calibration probes.

SPHERE—CONE TANGENT POINT (T.P.)

$\theta = 10°$

0.25-IN. RADIUS (R_n)

STAGNATION POINT (S.P.)
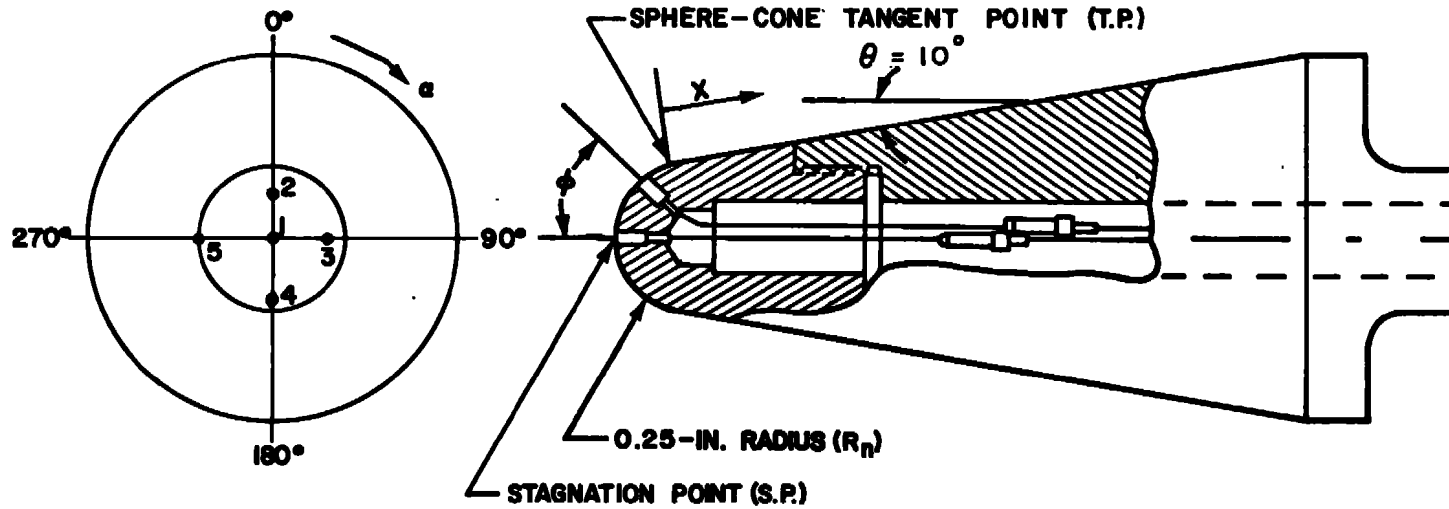
Calorimeter Slug	S/R_n	ϕ, deg	α, deg	X, in.
1	0	S.P.	S.P.	S.P.
2	1.050	60	0	N.A.
3	1.310	75	90	N.A.
4	3.375	80*	180	0.175*
5	3.800	80*	270	0.600*

*Slug located X distance downstream
of tangent point

NOTE: NOT TO SCALE

b. Calorimeter
Figure 8. Concluded.

GRAPHITE

1.00 8 UNC-3A
THREADS

0.5 R_n

2.5 DIAM

1/16 – DIAM
ORIFICE

3.25

"O" RING SEAL

TO TRANSDUCER

45°

2

HOLDER

ALL DIMENSIONS IN
INCHES
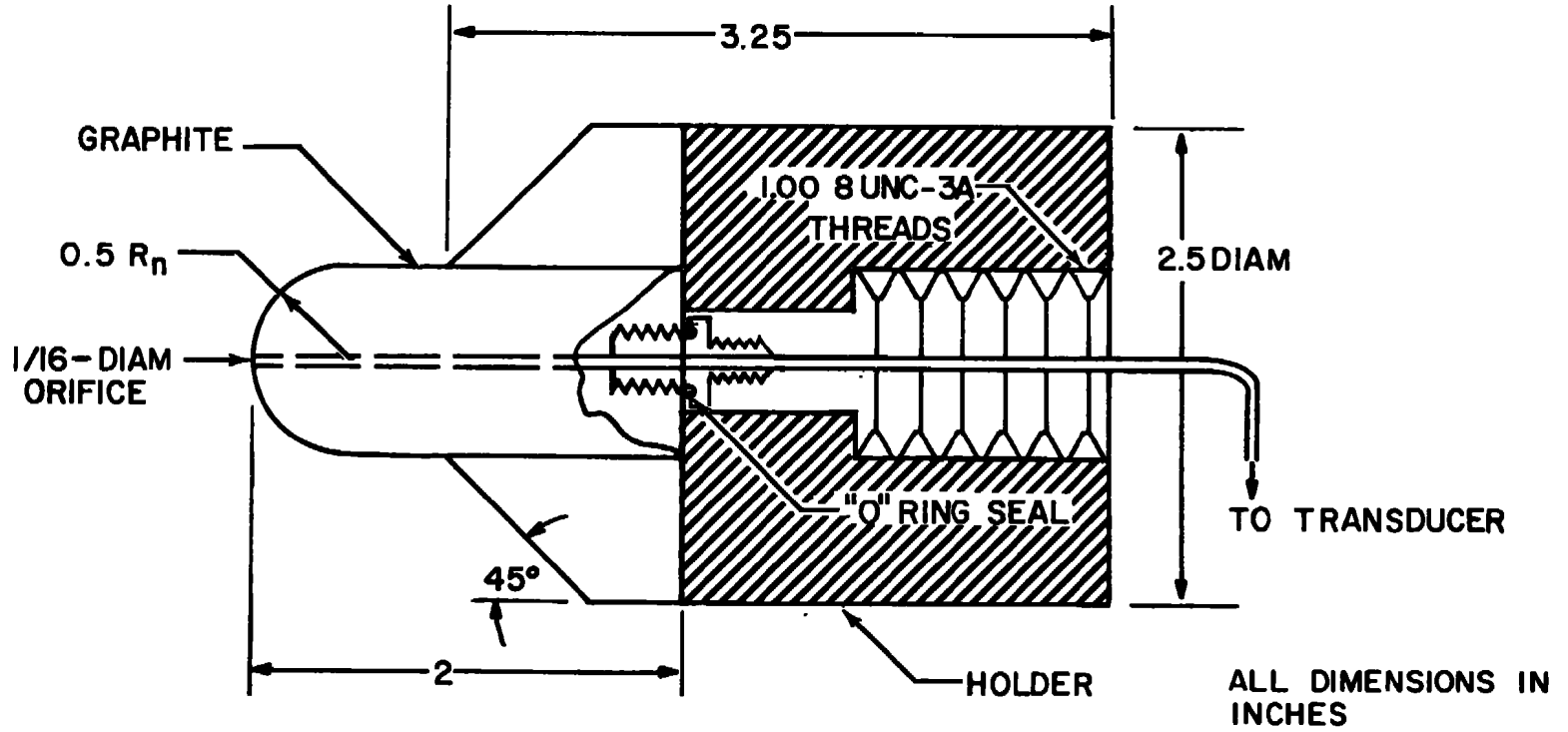
Figure 9. Axial pressure probe.
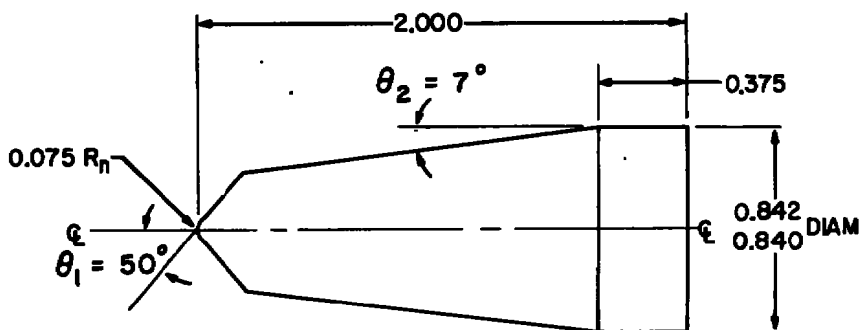
Cone-Cone (C)
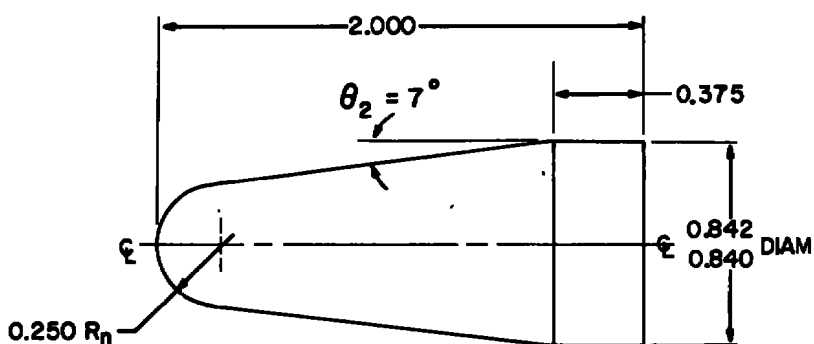
Sphere-Cone (S)
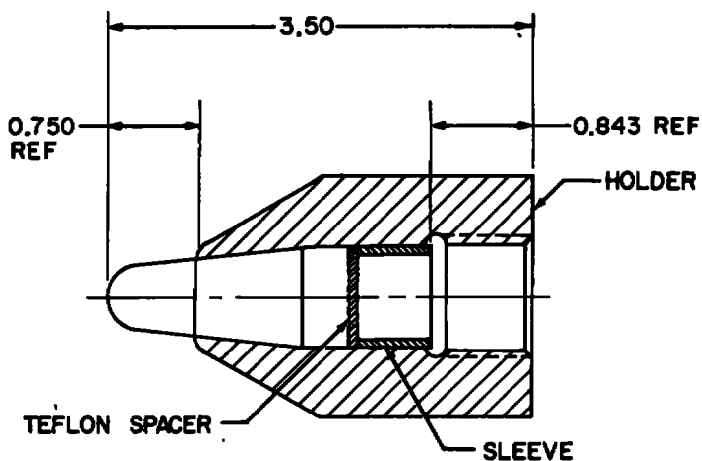
Model Assembly

ALL DIMENSIONS IN INCHES

Figure 10. Model configurations.

27
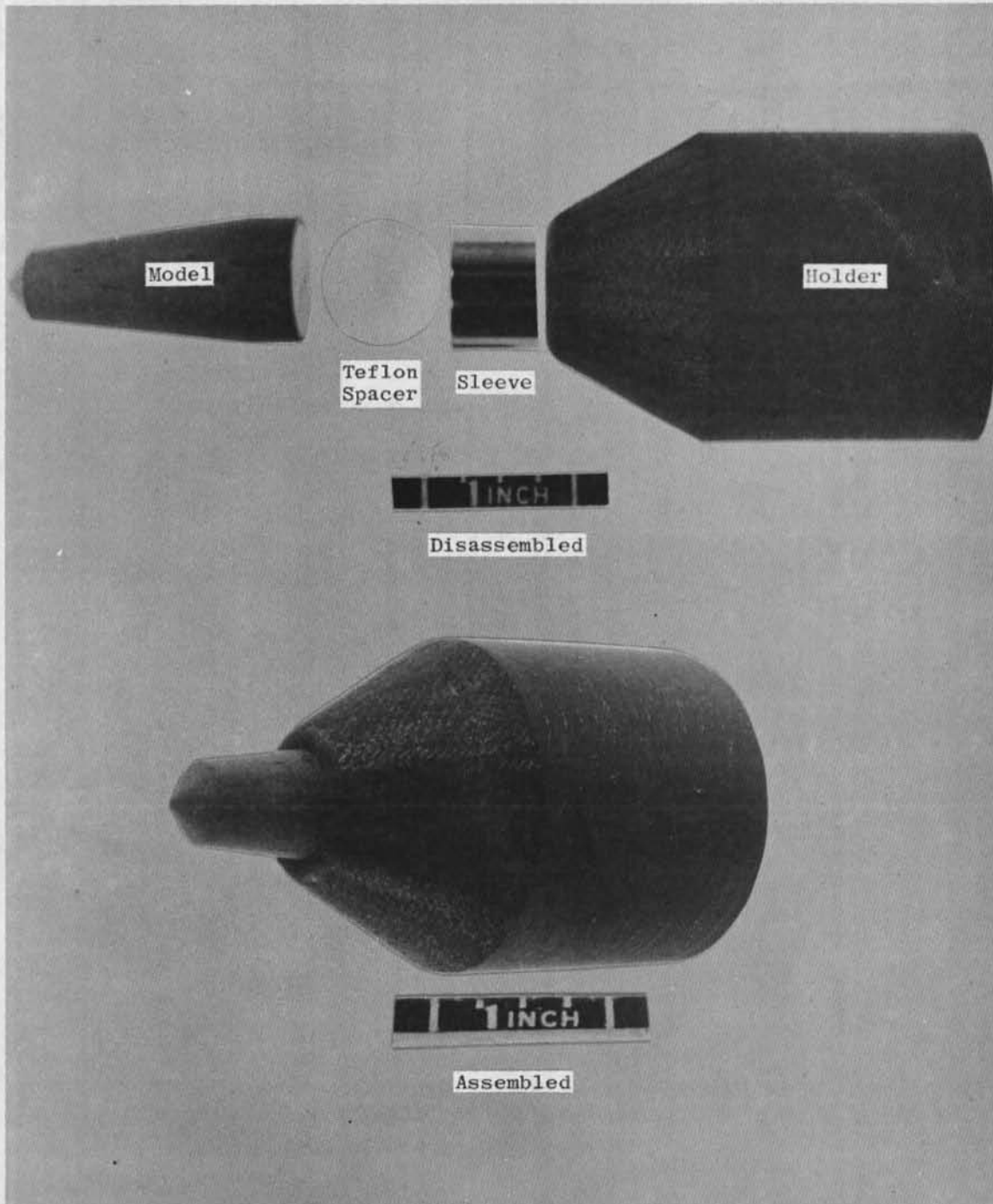
Figure 11. Model and holder.
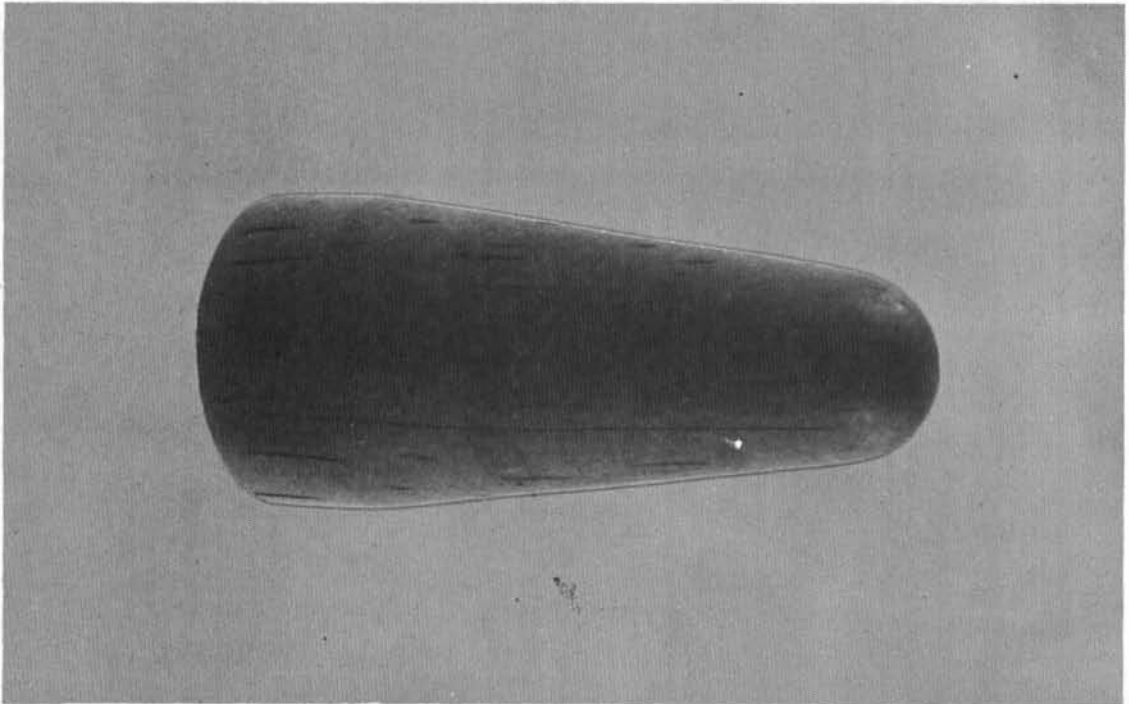
a. Sphere-cone
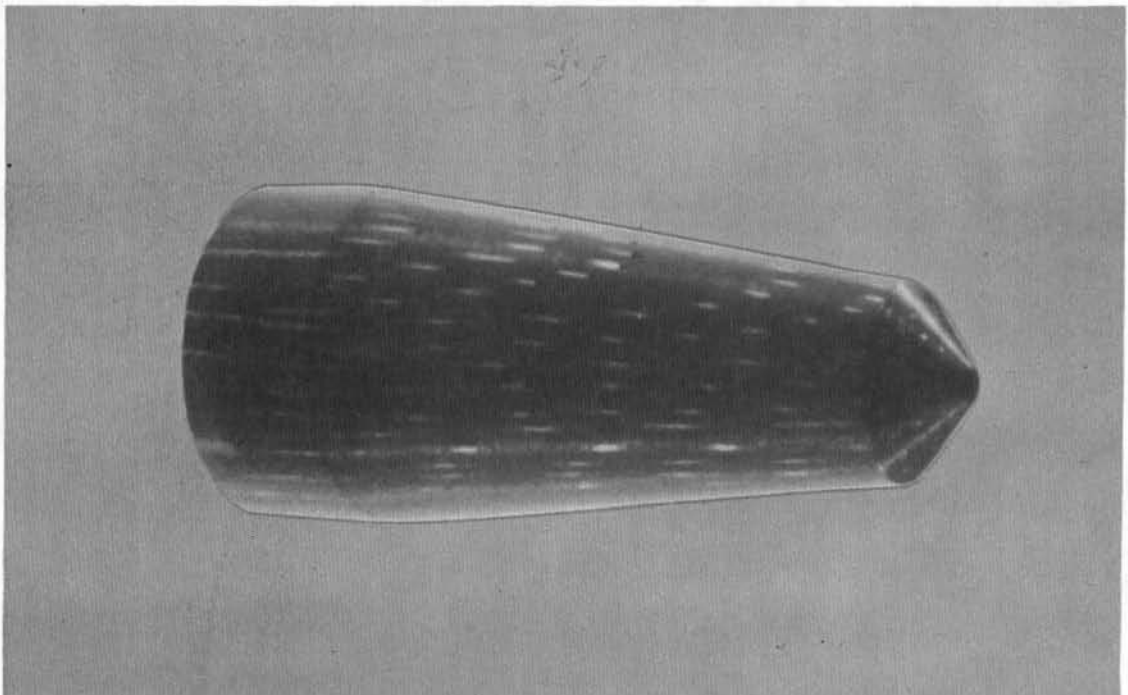
b. Cone-cone
Figure 12. Typical model pretest photograph.

Sweep Made 0.1 in. from
Nozzle Exit at 25 in./sec
See Fig. 8a for Probe Details

RUN 8

M = 2.0

NOZZLE WALL

0.255

$p_o' / p_{o_{\mathcal{C}}}'$

p_o = 142.24 atm

$p_{o_{\mathcal{C}}}'$ = 92.83 atm

H_o = 2302 Btu/lbm

RADIAL POSITION, inches
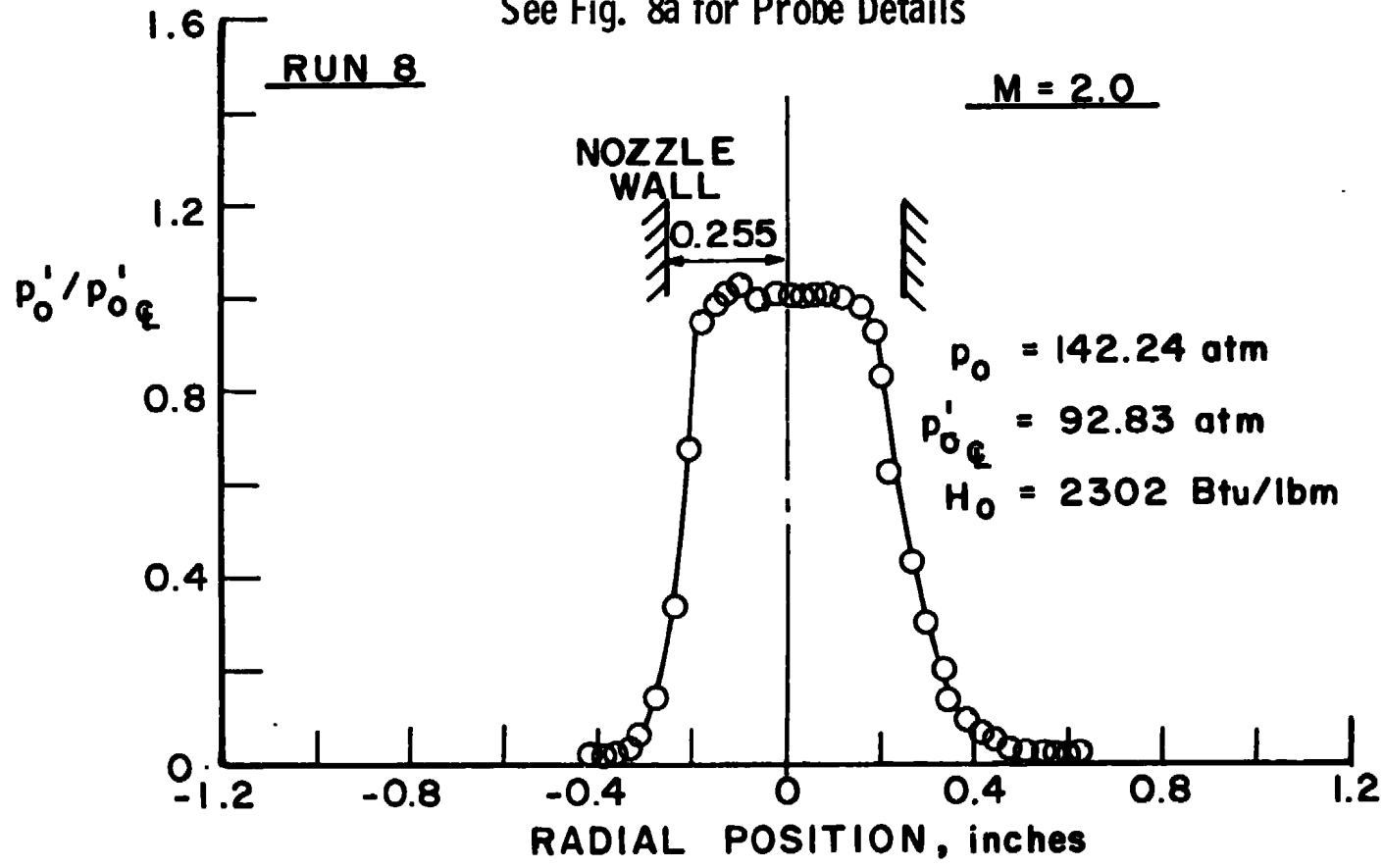
Figure 13. Radial impact pressure ratio profiles obtained with conventional
Mach number 2.0 nozzle.
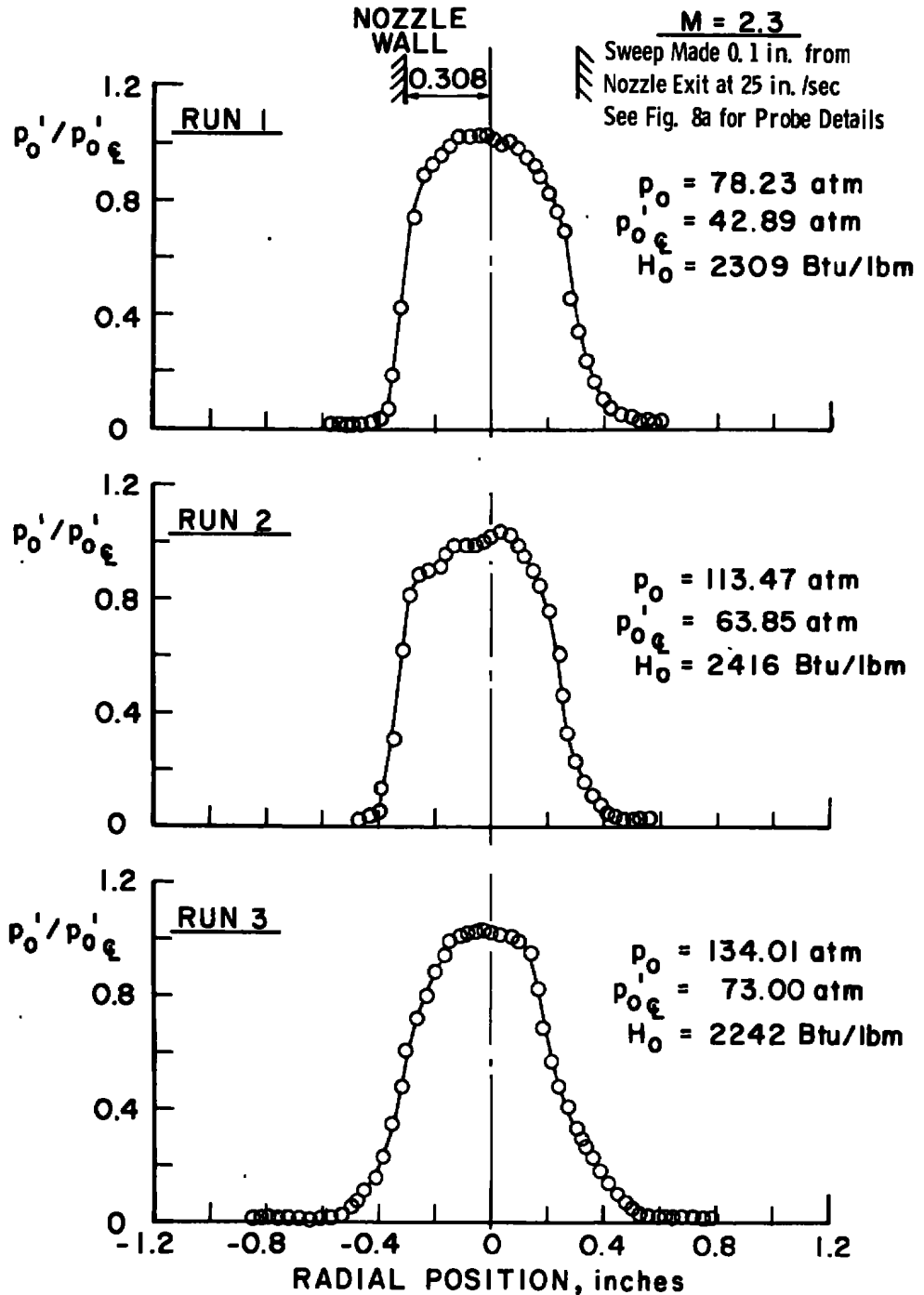
Figure 14. Radial impact pressure ratio profiles obtained with conventional Mach number 2.3 nozzle.
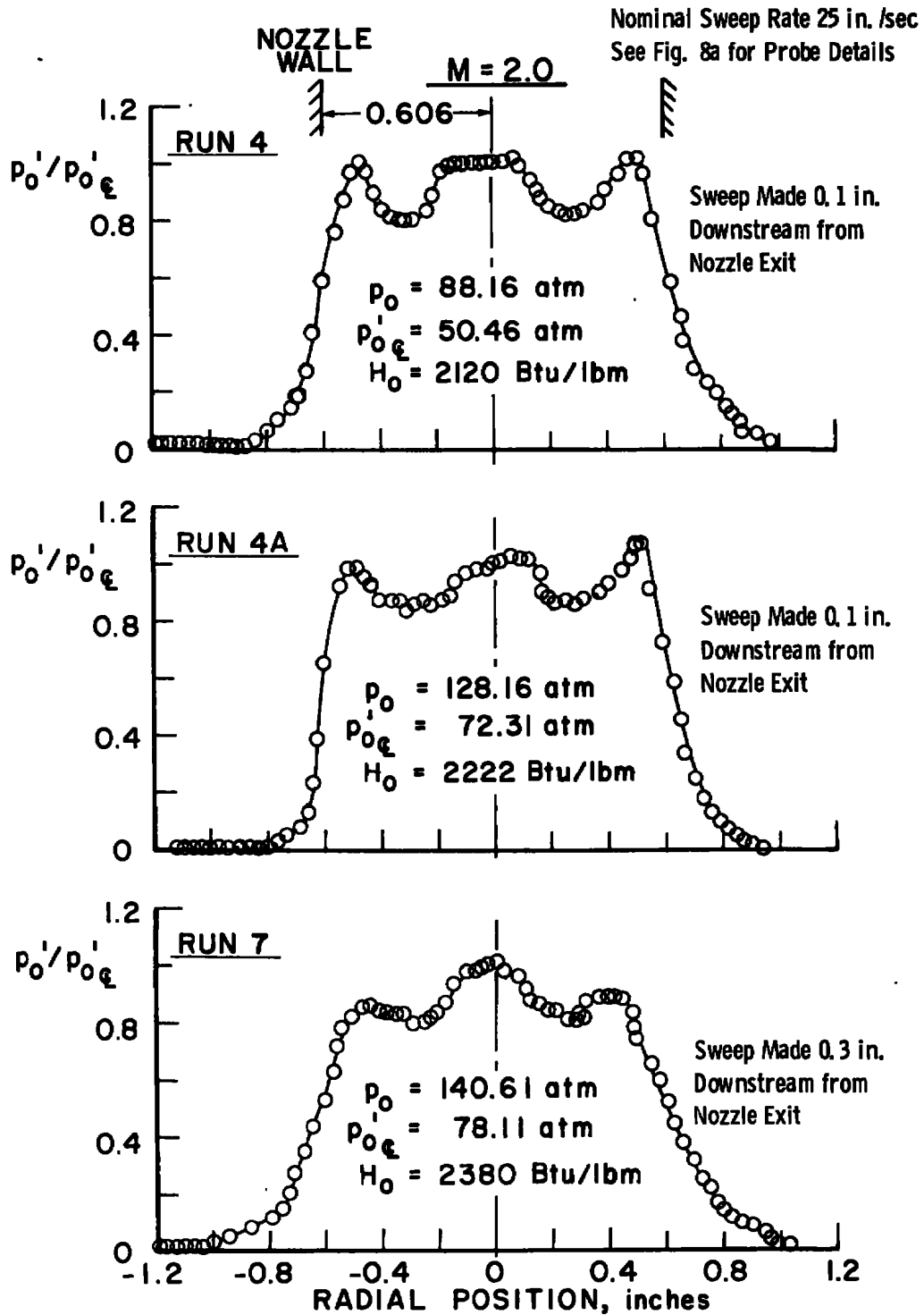
Figure 15. Radial impact pressure ratio profiles obtained with internal cold shroud nozzle, Mach number 2.0.
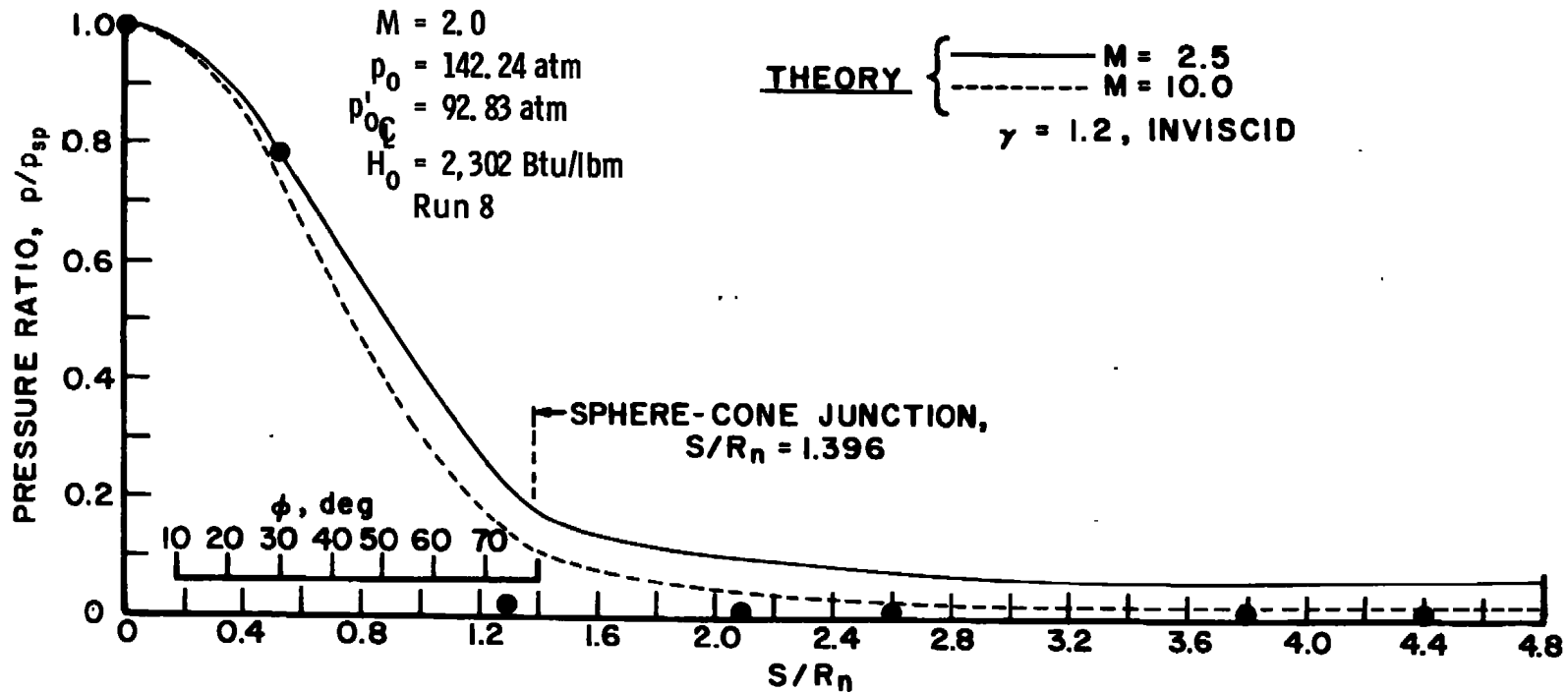
a. Mach 2.0
Figure 16. Comparison of measured sphere-cone pressure ratios obtained with conventional nozzles and calculated inviscid values.

M = 2.3

Sym	Run	p_0, atm	p'_{0_C}, atm	H_0, Btu/lbm
●	1	78.23	42.89	2,309
■	2	113.47	63.85	2,416
▲	3	134.01	73.00	2,242

THEORY { —————— M = 2.5
        { - - - - - - M = 10.0

γ = 1.2, INVISCID

SPHERE-CONE JUNCTION,
S/R_n = 1.396

ϕ, deg
10 20 30 40 50 60 70

PRESSURE RATIO, p/p_{sp}

S/R_n
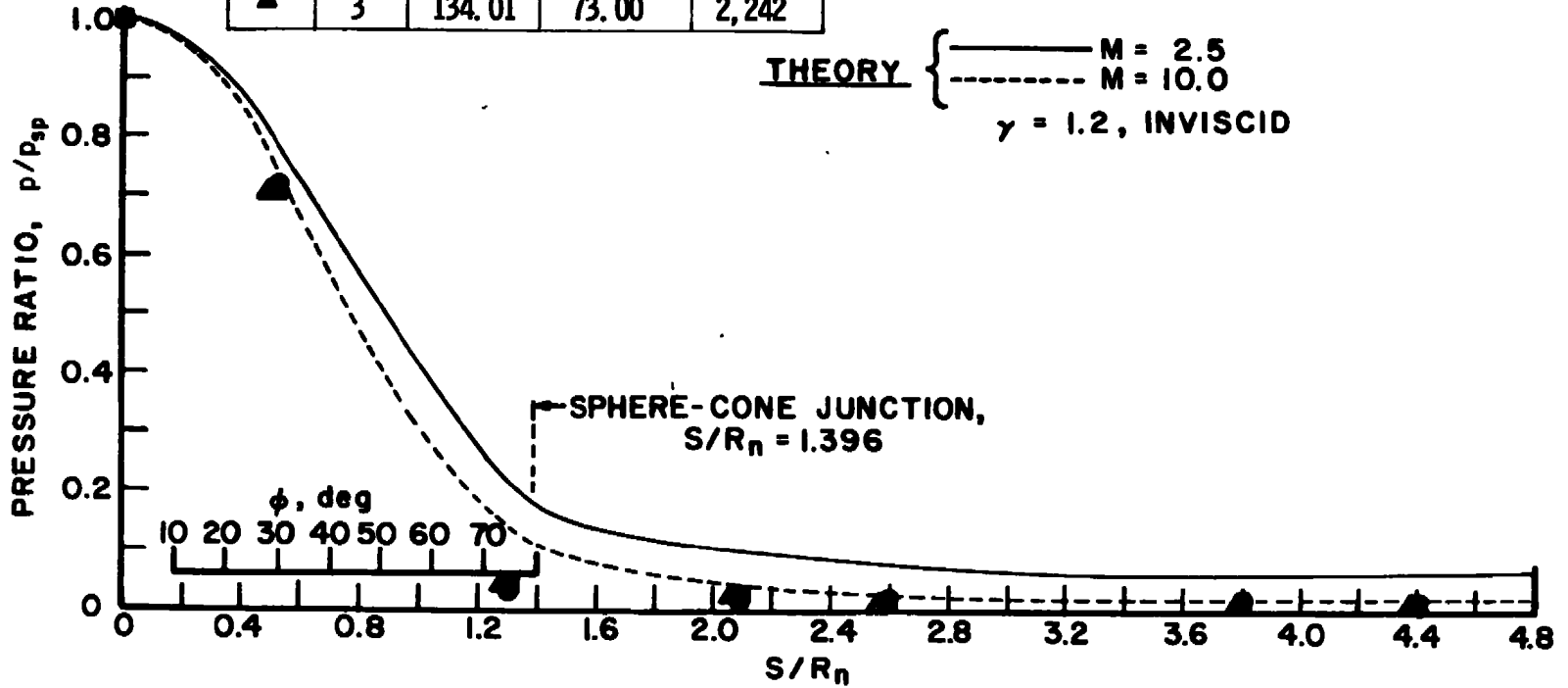
b. Mach 2.3
Figure 16. Concluded.

M = 2.0

Sym	Run	p_{0}, atm	p'_{0_C}, atm	H_{0}, Btu/lbm
●	4	88. 16	50. 46	2, 120
■	4A	128. 16	72. 31	2, 222
▲	7	140. 61	78. 11	2, 380

THEORY
M = 2.5
------- M = 10.0
γ = 1.2 , INVISCID

SPHERE-CONE JUNCTION,
S/R_n = 1.396

ϕ, deg
10 20 30 40 50 60 70

PRESSURE RATIO, p/p_{sp}

S/R_n
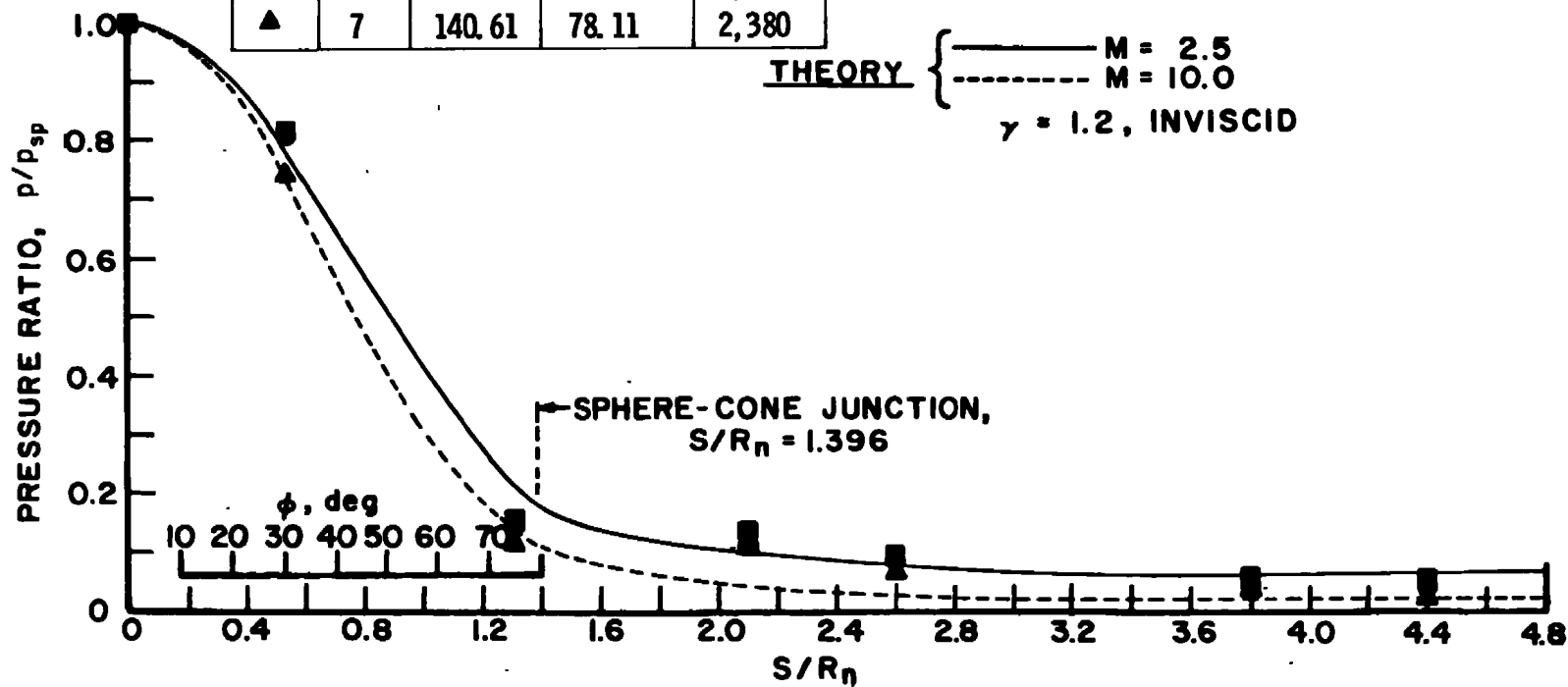
Figure 17. Comparison of measured sphere-cone pressure ratios obtained with internal cold
shroud nozzle and calculated inviscid values.
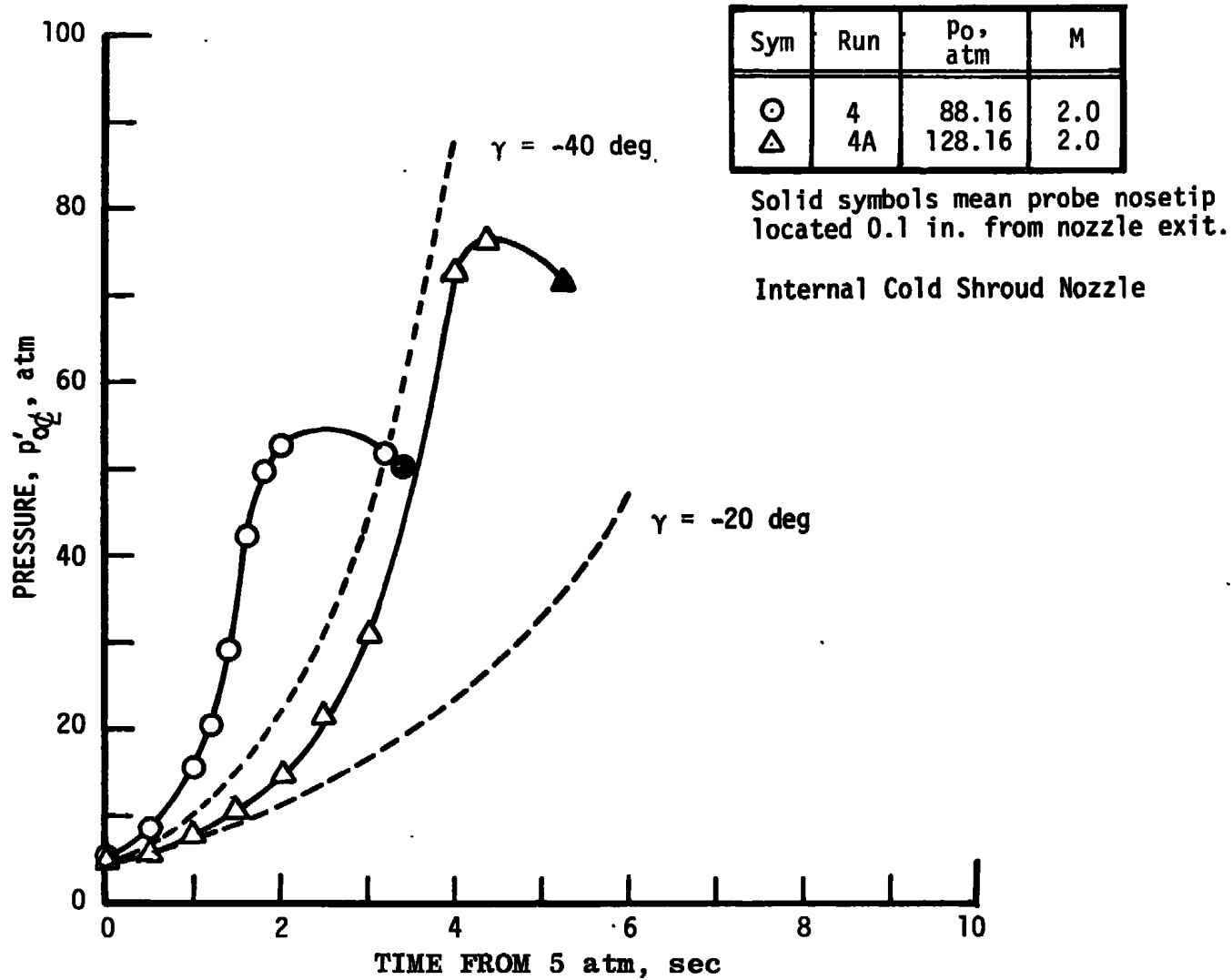
Figure 18. Typical reentry pressure histories at -20- and -40-deg entry angles and comparison with two axial traverses.
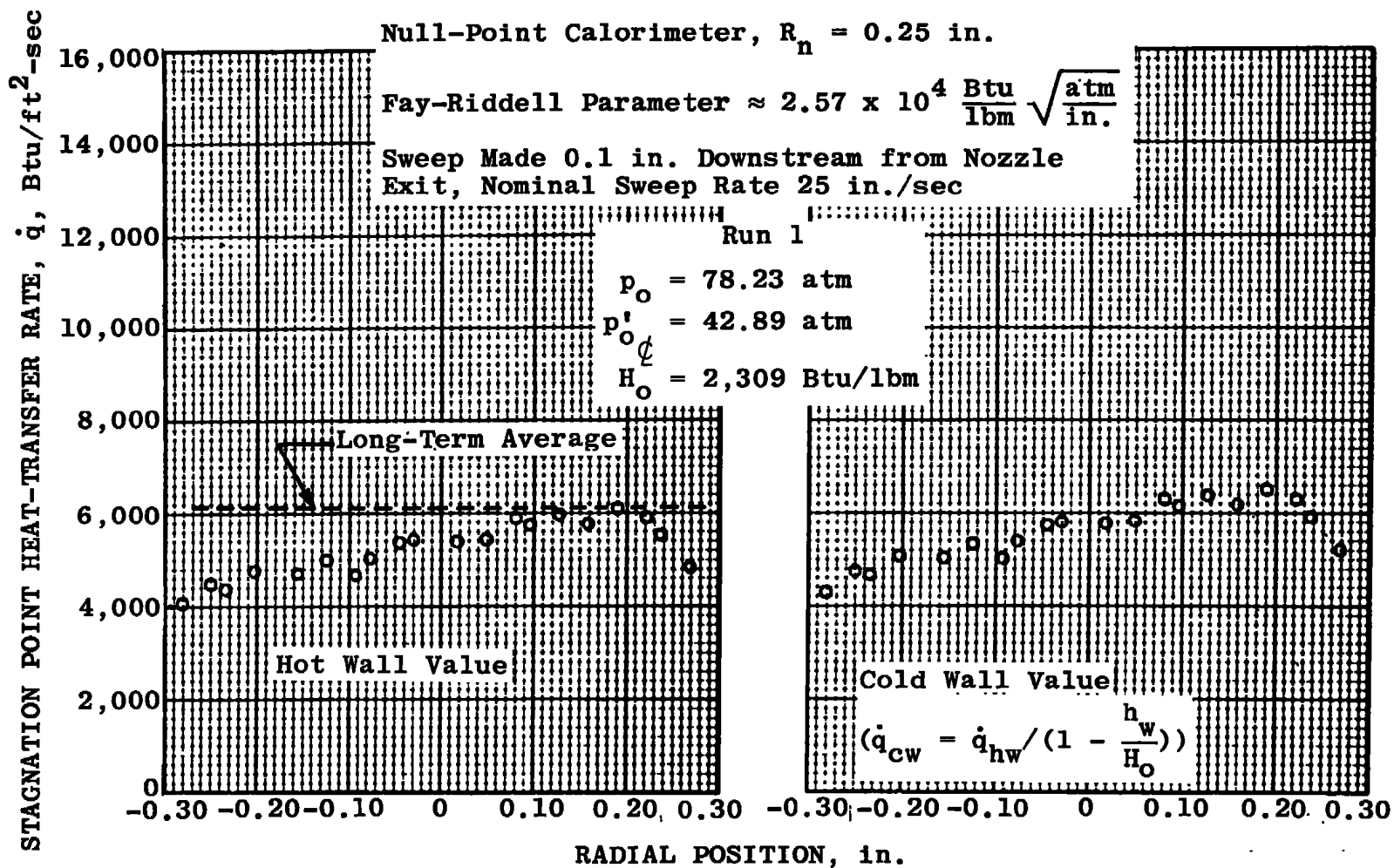
a. Mach 2.3 conventional nozzle, run 1
Figure 19. Radial profiles of heat-transfer rates.
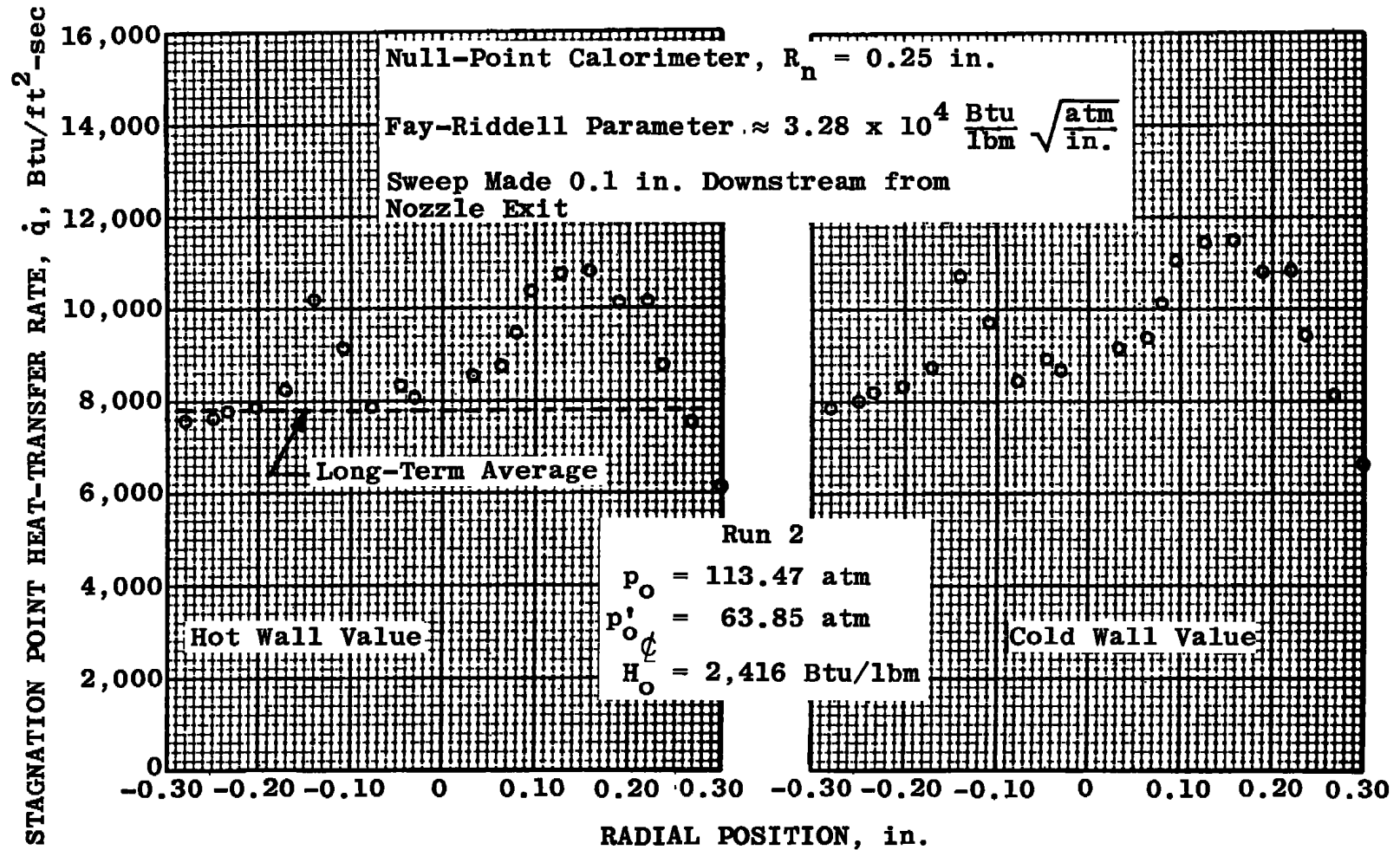
b. Mach 2.3 conventional nozzle, run 2
Figure 19. Continued.

STAGNATION POINT HEAT-TRANSFER RATE, $\dot{q}$, Btu/ft^2-sec

Null-Point Calorimeter, R_n = 0.25 in.

Fay-Riddell Parameter $\approx 3.26 \times 10^4 \frac{Btu}{lbm} \sqrt{\frac{atm}{in.}}$

Sweep Made 0.1 in. Downstream from Nozzle Exit

Long-Term Average

Run 3

p_o = 134.0 atm

p_o' = 73.0 atm

H_o = 2,242 Btu/lbm

Hot Wall Value

Cold Wall Value

RADIAL POSITION, in.
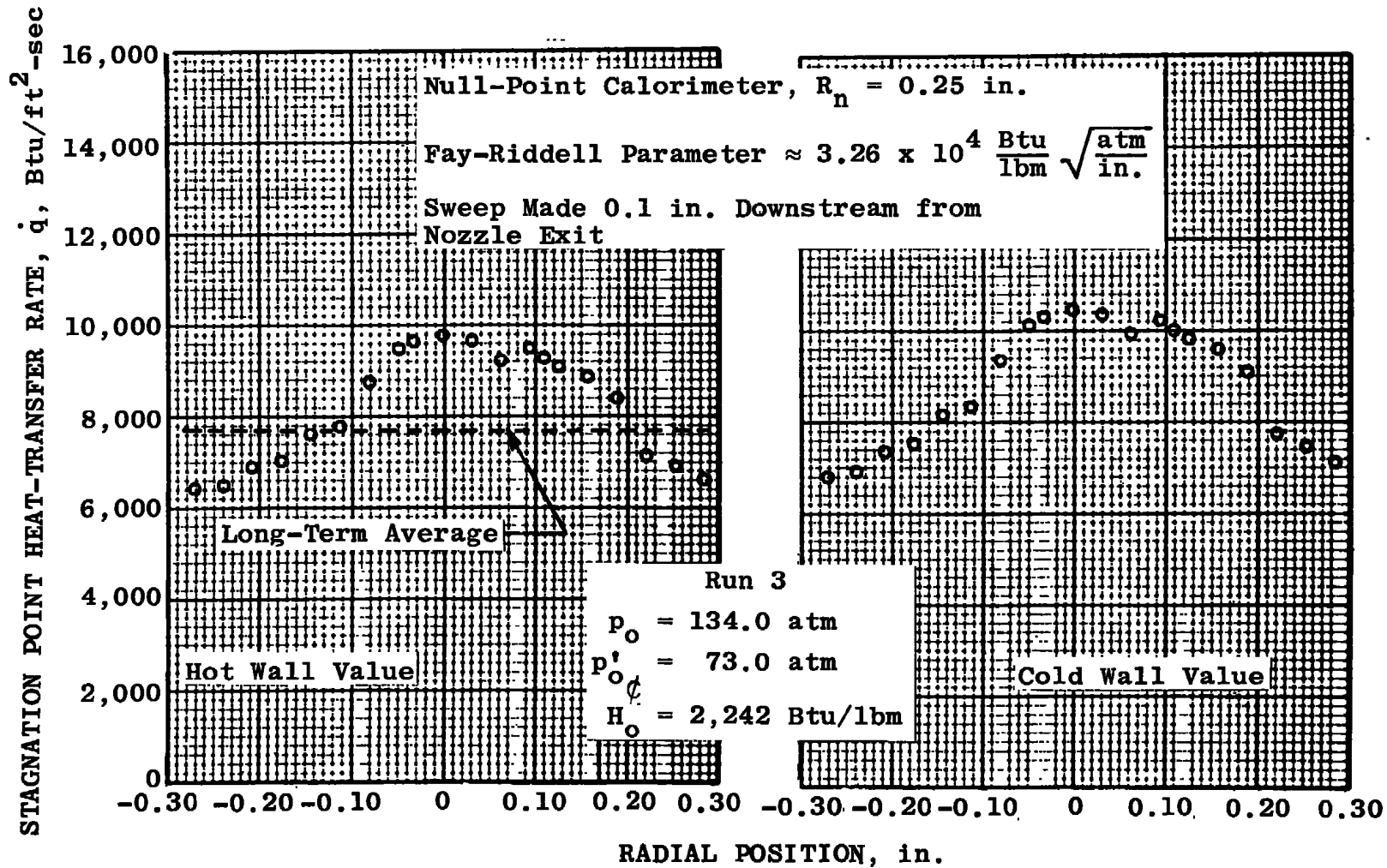
c. Mach 2.3 conventional nozzle, run 3
Figure 19. Continued.
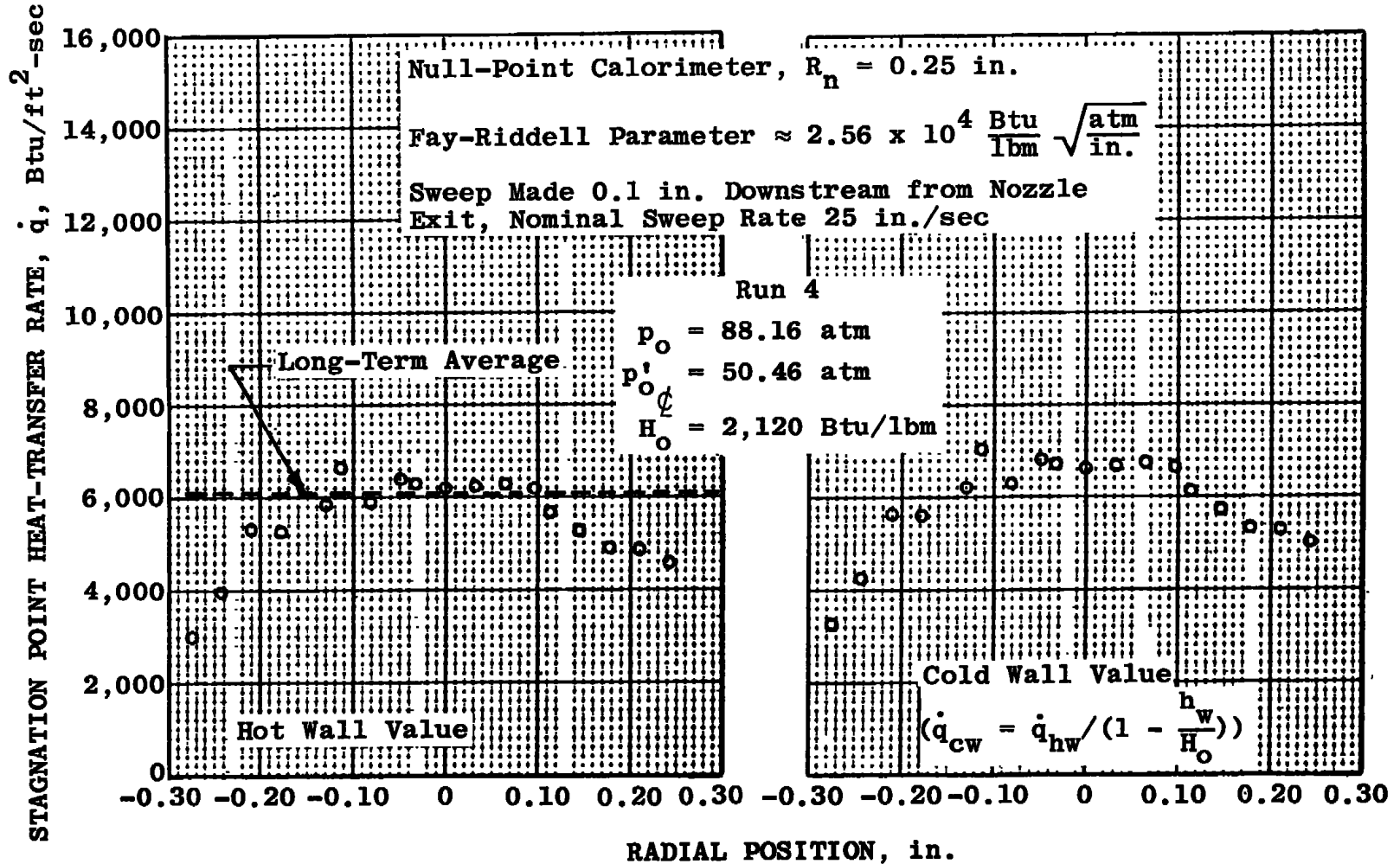
d. Mach 2.0 ICS nozzle, run 4
Figure 19. Continued

Within the figure:

Null-Point Calorimeter, $R_n = 0.25$ in.

Fay-Riddell Parameter $\approx 2.56 \times 10^4 \frac{Btu}{lbm} \sqrt{\frac{atm}{in.}}$

Sweep Made 0.1 in. Downstream from Nozzle Exit, Nominal Sweep Rate 25 in./sec

Run 4
$p_o = 88.16$ atm
$p_o' = 50.46$ atm
$H_o = 2,120$ Btu/lbm

Long-Term Average

Hot Wall Value

Cold Wall Value
$(\dot{q}_{cw} = \dot{q}_{hw}/(1 - \frac{h_w}{H_o}))$

STAGNATION POINT HEAT-TRANSFER RATE, $\dot{q}$, Btu/ft^2-sec

RADIAL POSITION, in.
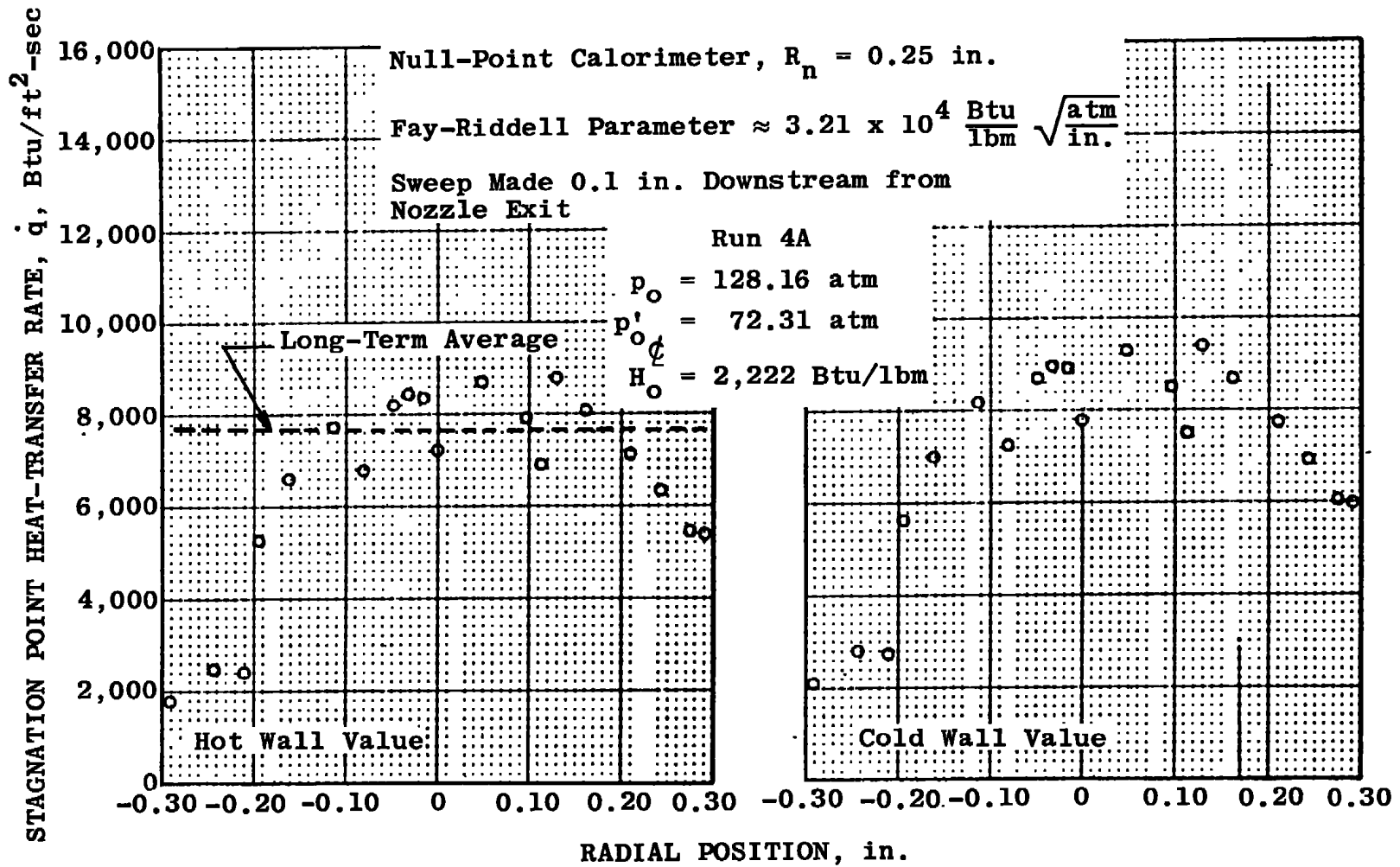
e. Mach 2.0 ICS nozzle, run 4A
Figure 19. Continued.
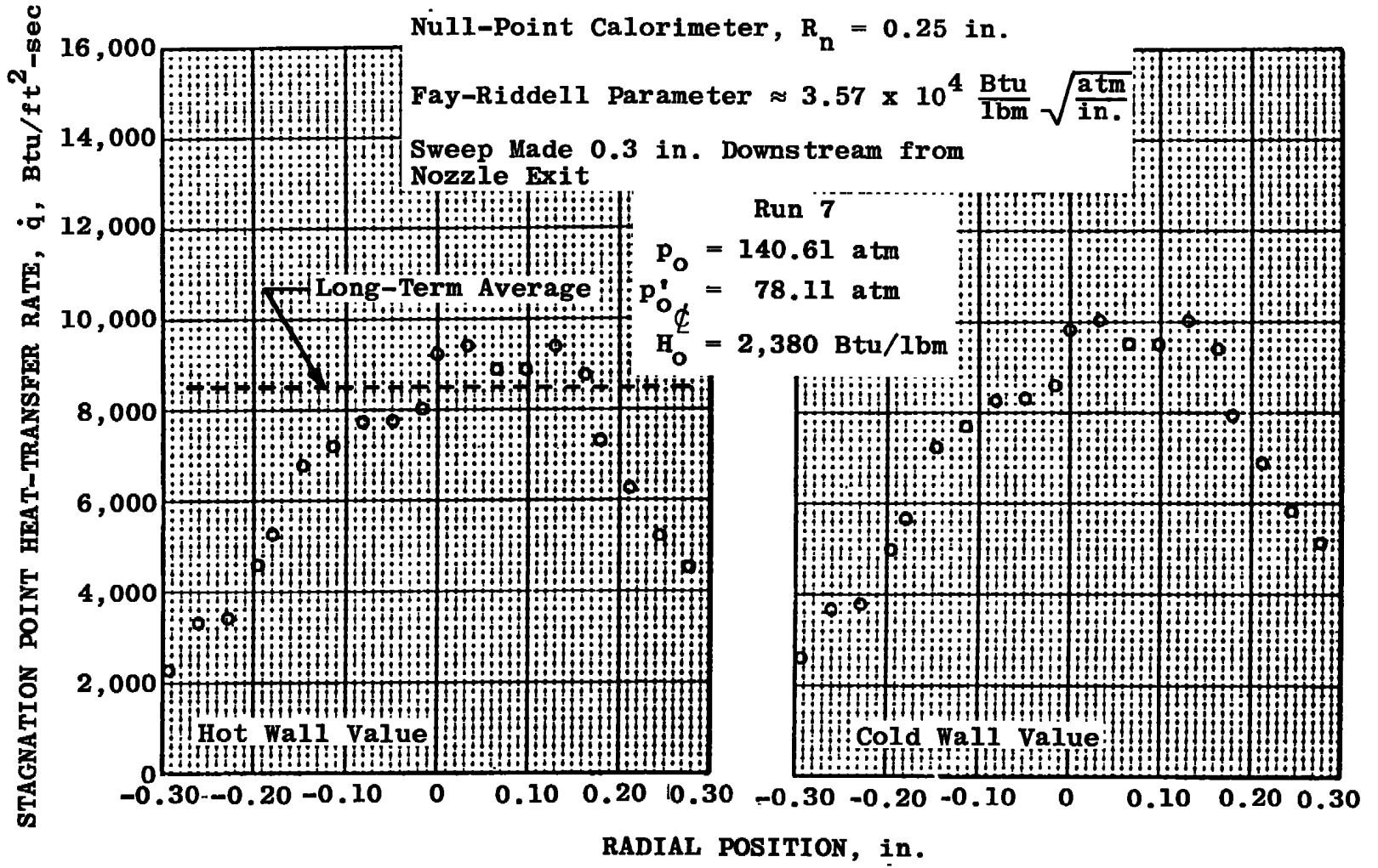
f. Mach 2.0 ICS nozzle, run 7
Figure 19. Continued.
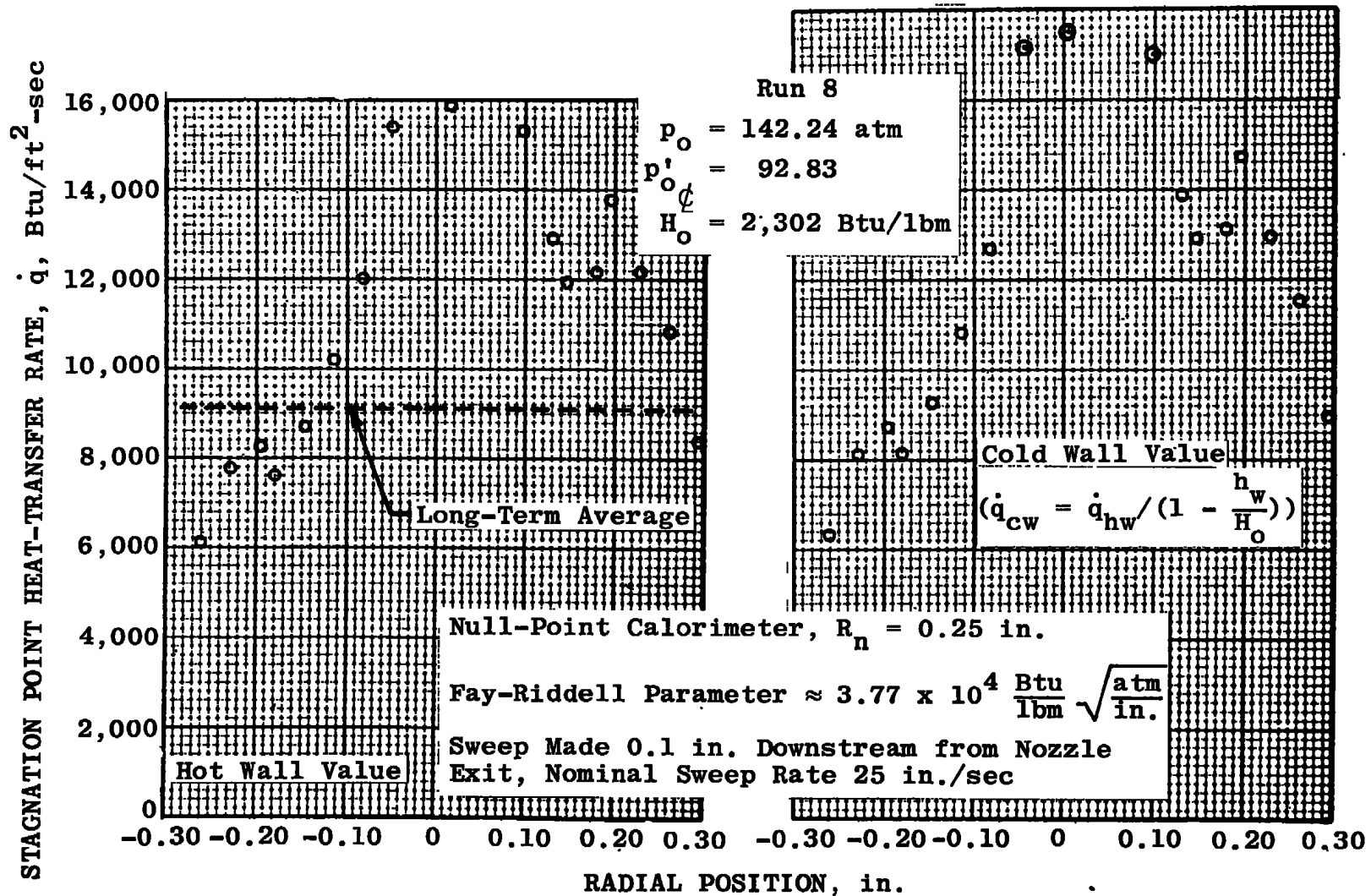
g. Mach 2.0 conventional nozzle, run 8
Figure 19. Concluded.
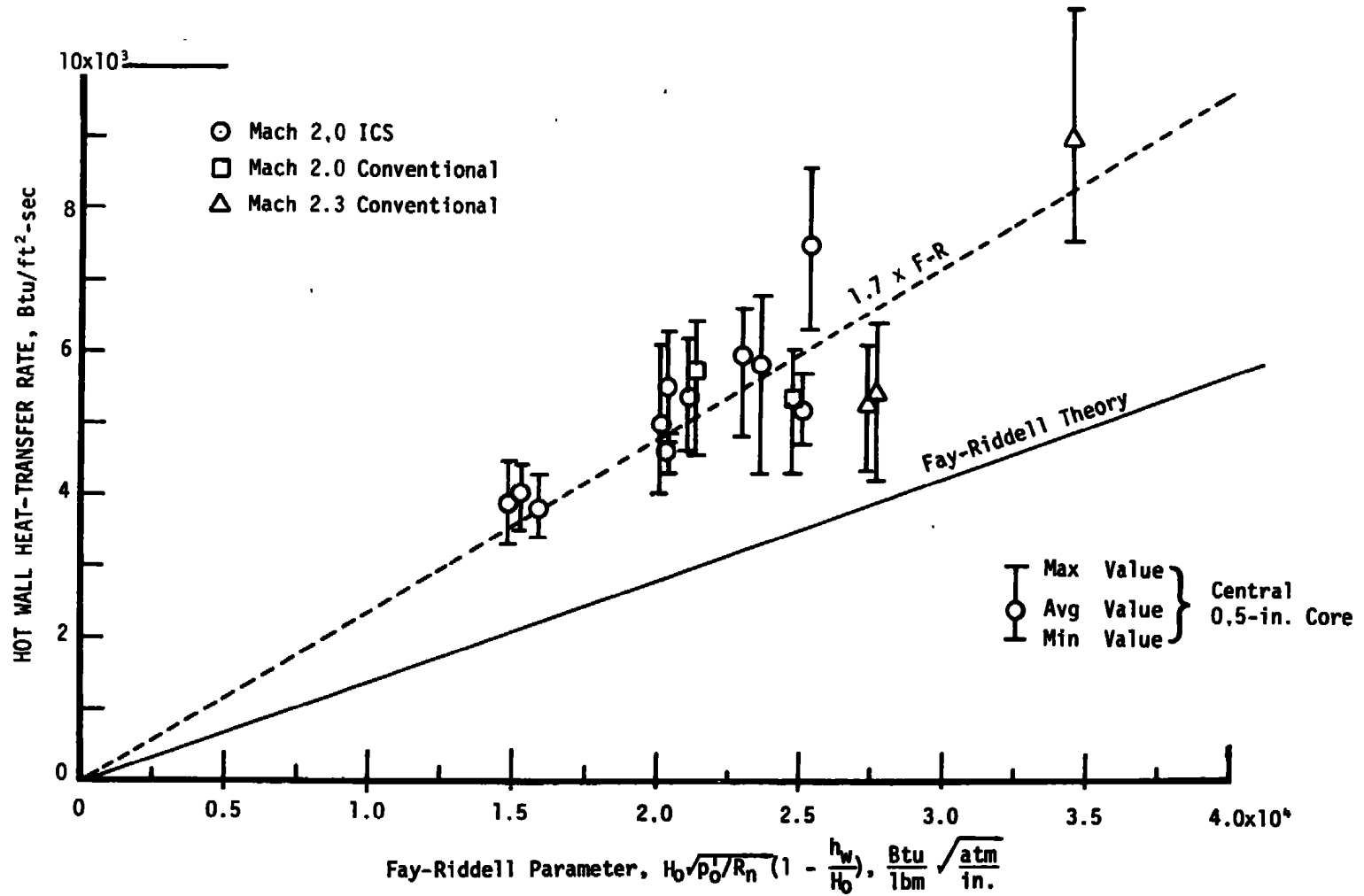
Figure 20. Long-term heat-transfer rates.

A11-S   A21-S

A31-S   A41-S
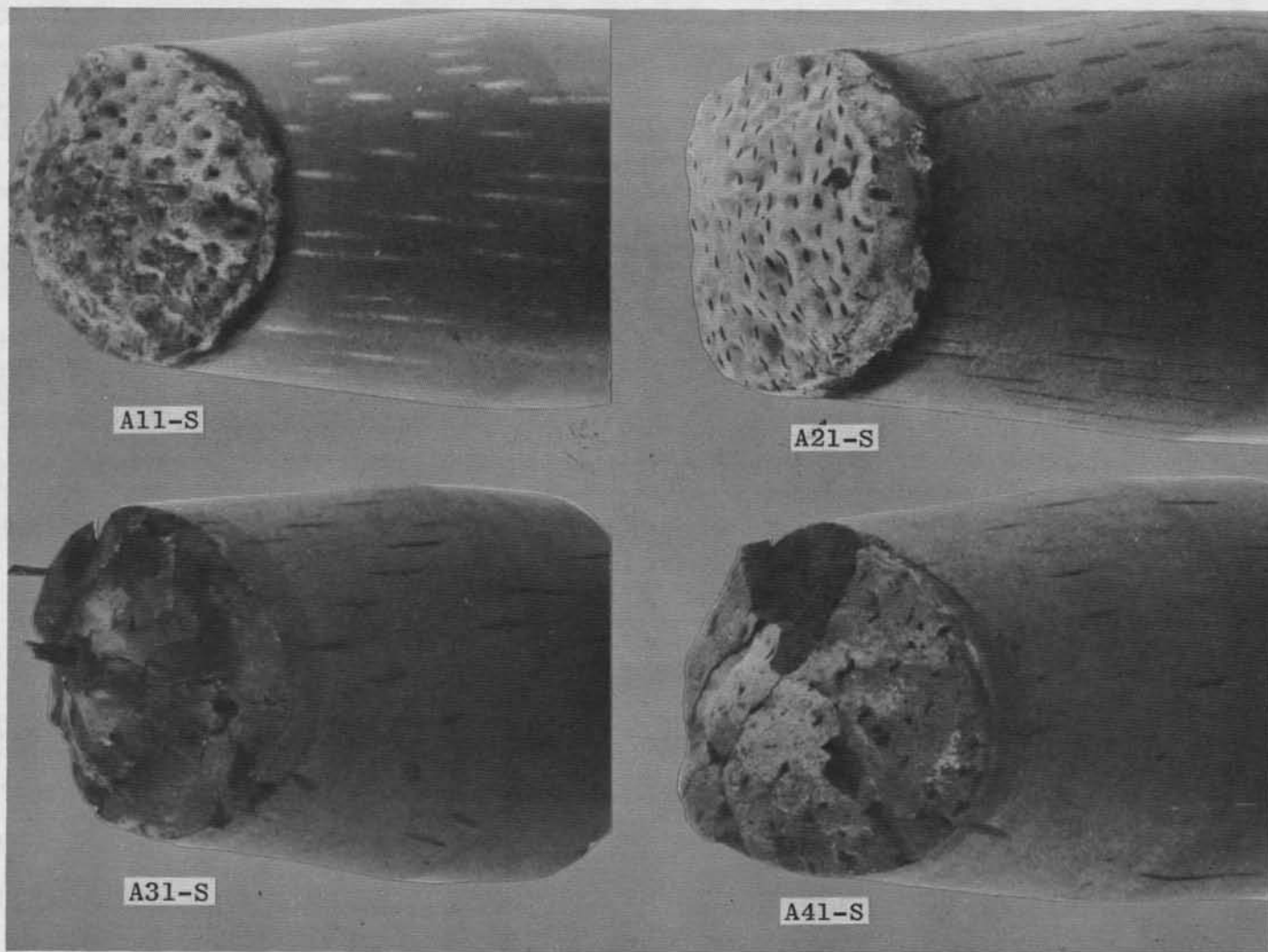
a. Run 1

Figure 21. Model posttest photographs.
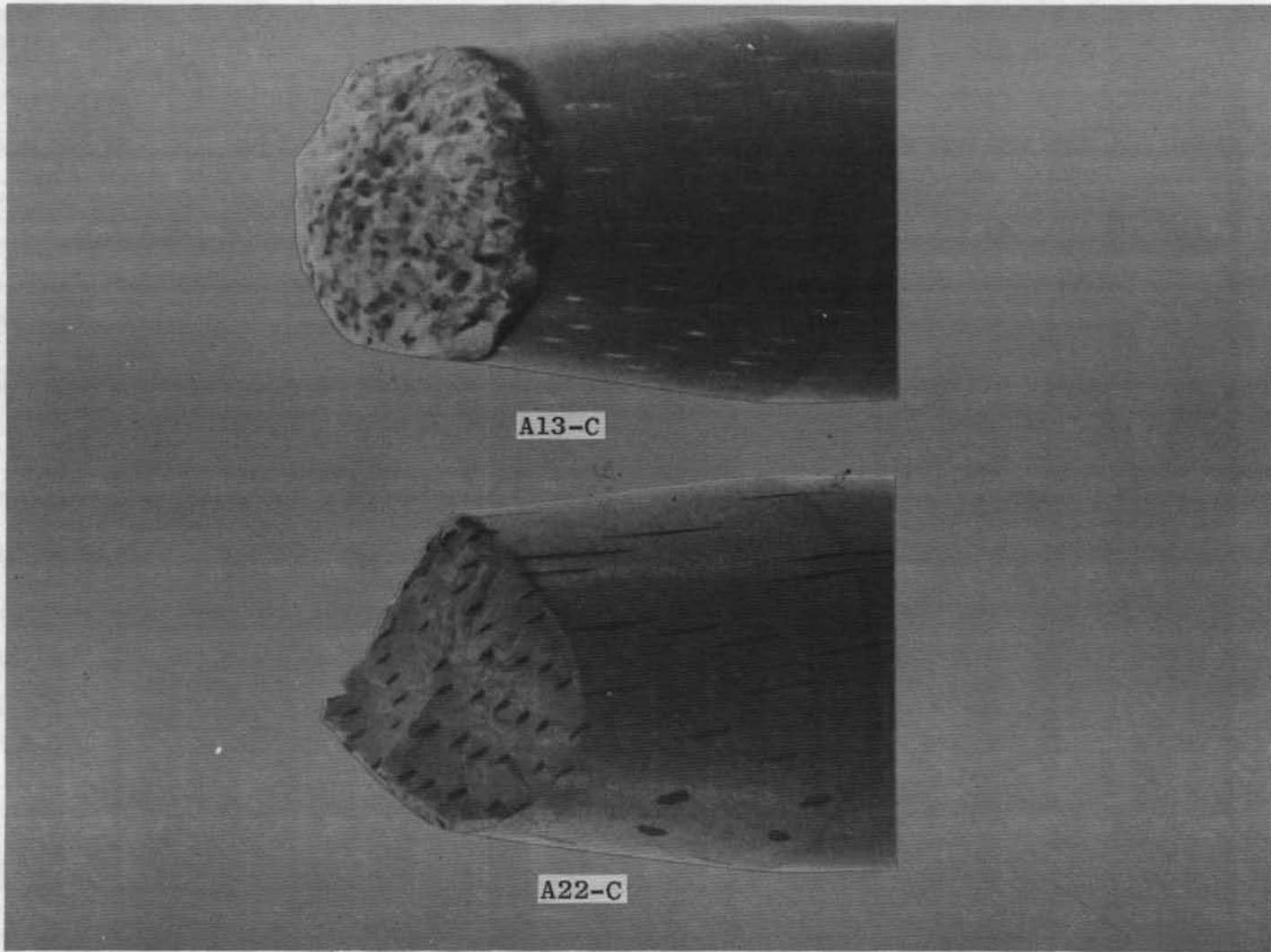
A13-C

A22-C

b. Run 2
Figure 21. Continued.

A15-C

A32-C

A44-C

8S-12-1
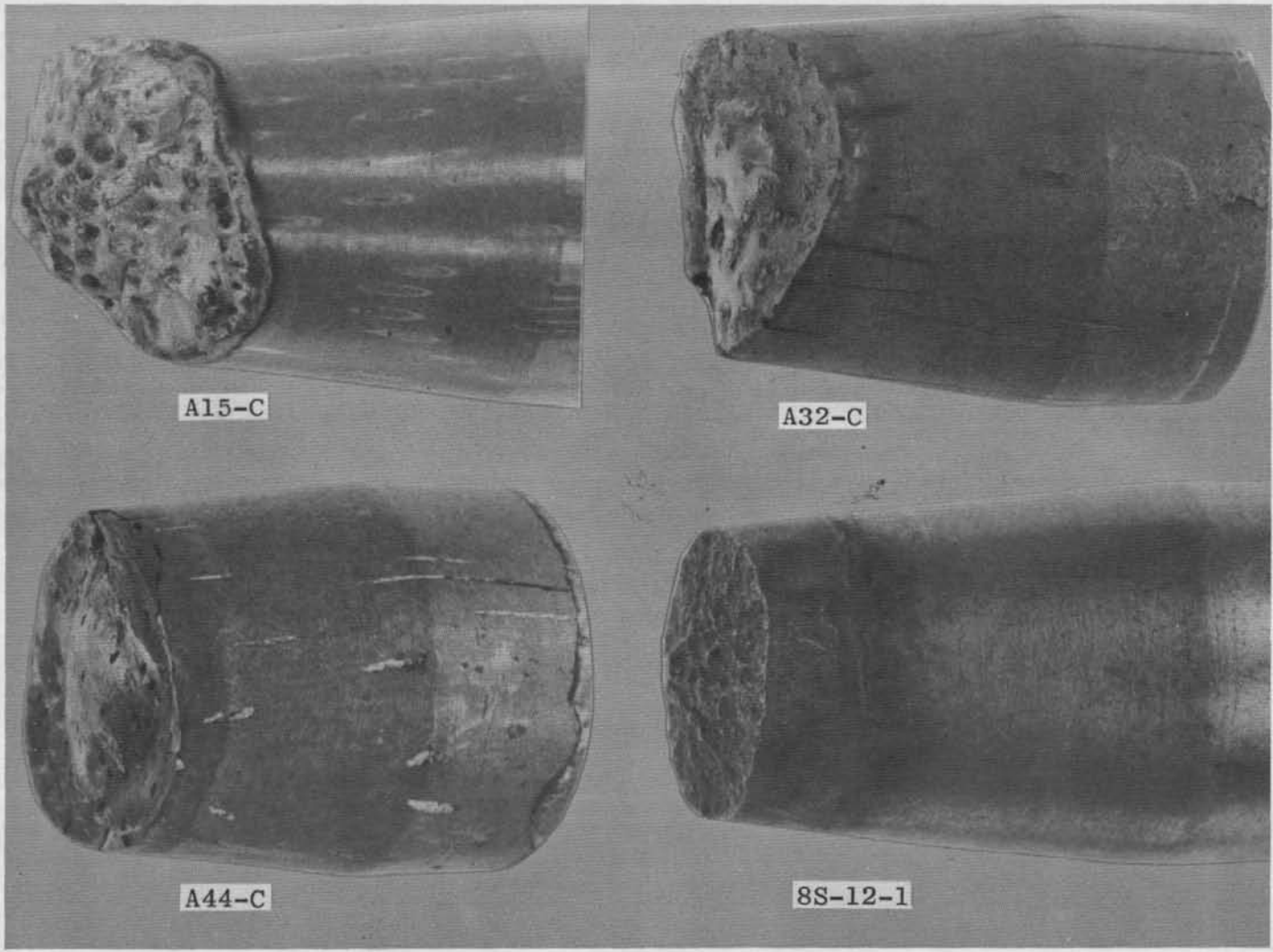
c. Run 3
Figure 21. Continued.
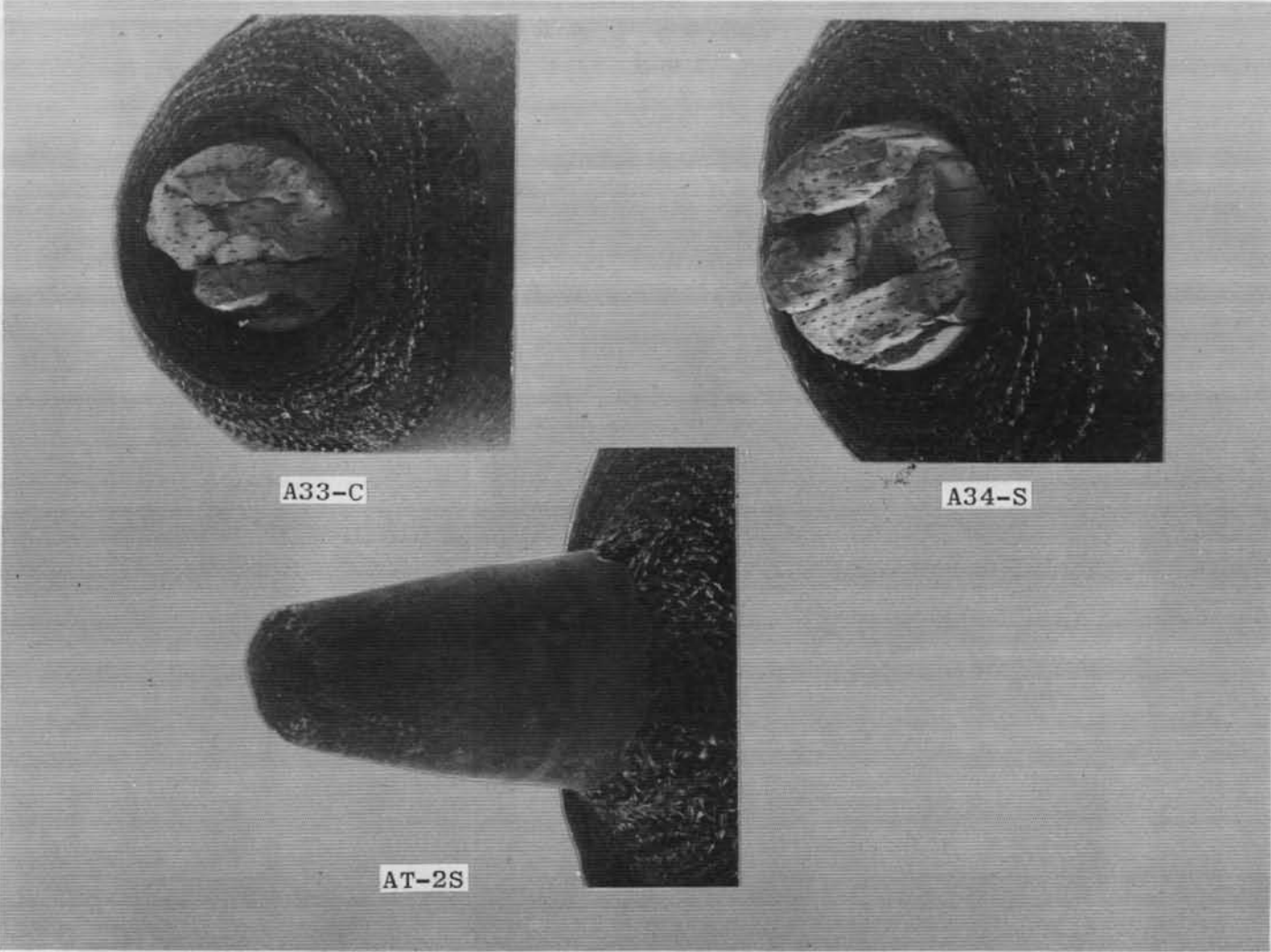
A33-C

A34-S

AT-2S

d. Run 5
Figure 21. Continued.

A12-S

C11-S

A45-C
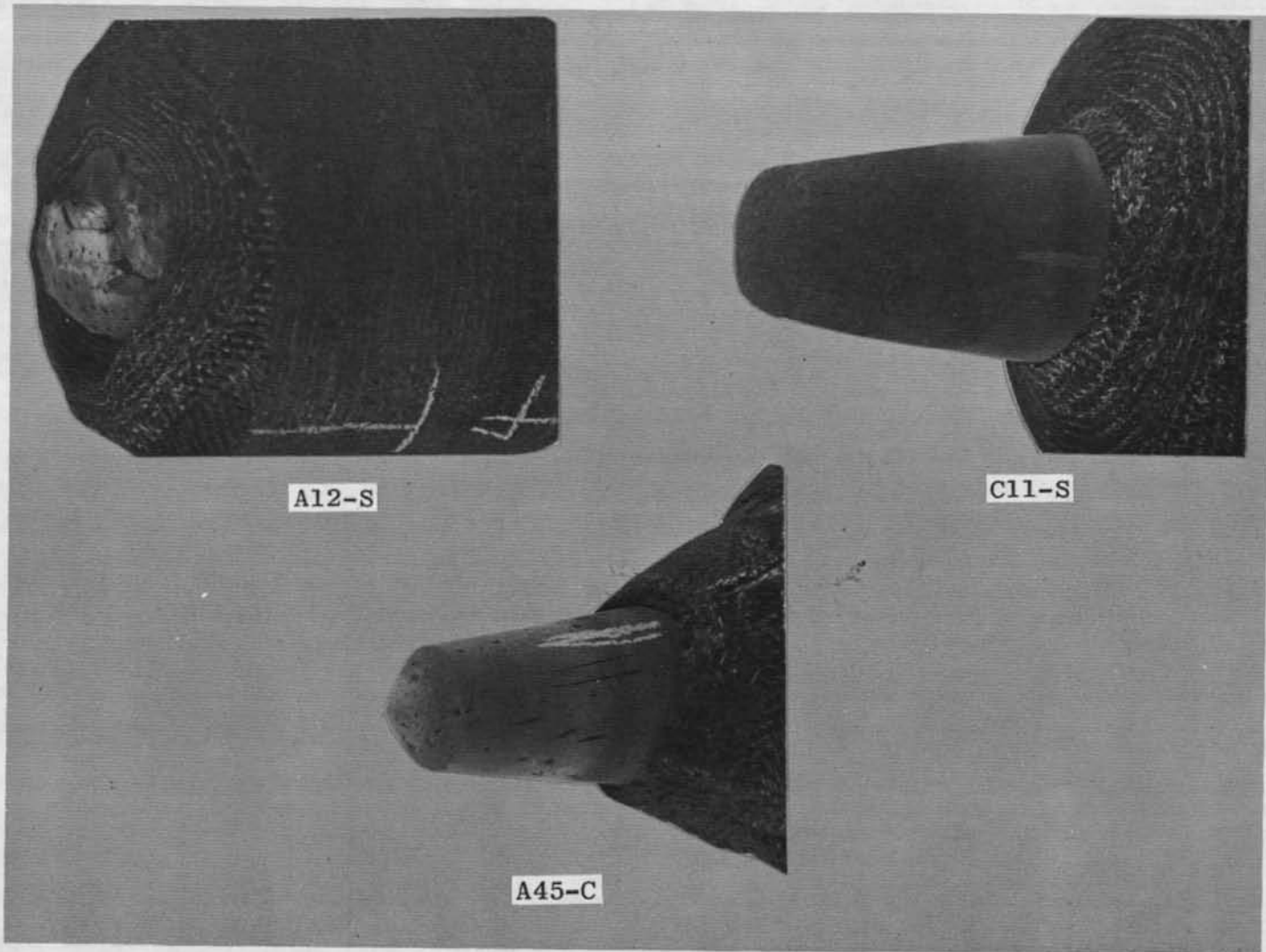
e. Run 6
Figure 21. Continued.

49
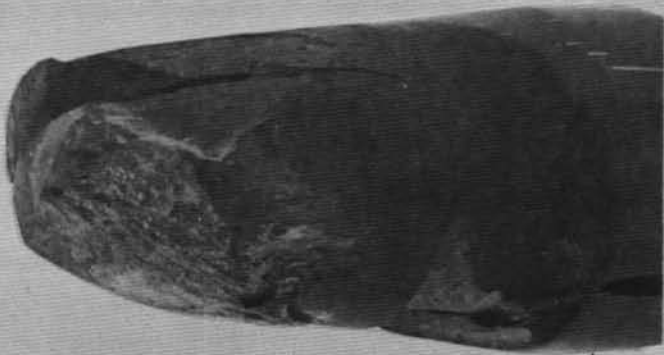
A42-S
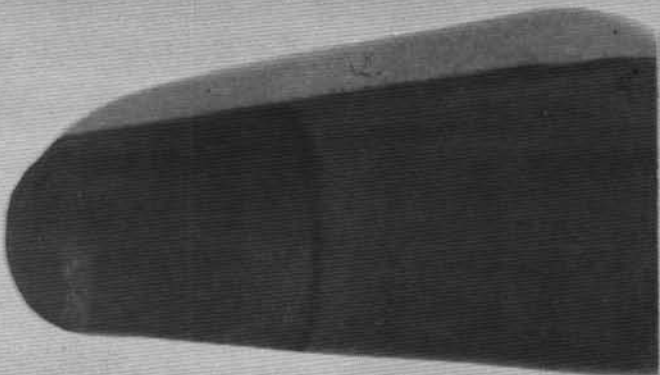
C11-C

f. Run 7
Figure 21. Continued.

A14-C

A23-C

A16-S

8S-12-2
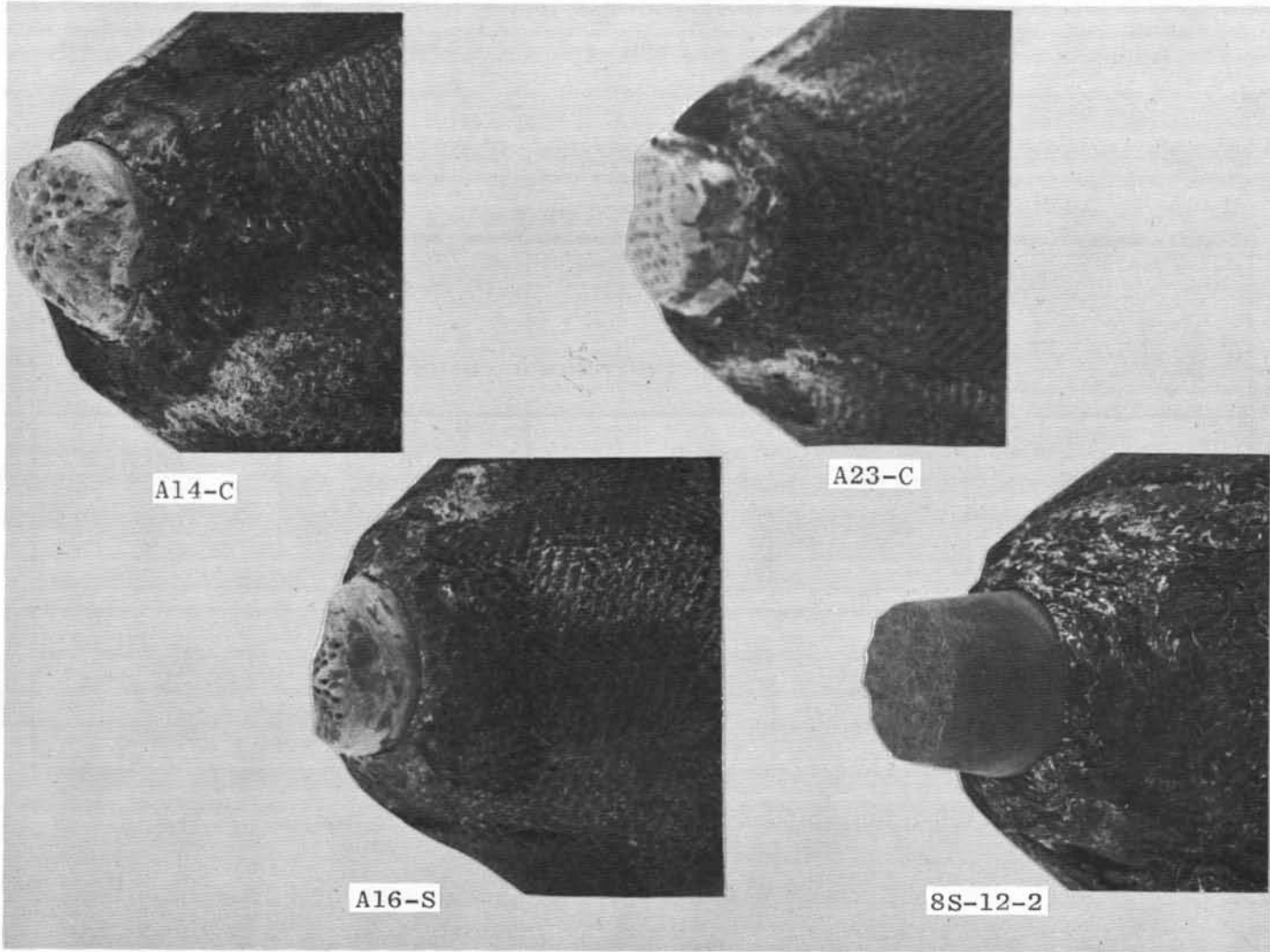
g. Run 8
Figure 21. Concluded.

Table 1. Nozzles Available in Arc Heater Test Unit (5 MW)

Nominal Exit Mach Number	Throat Diameter, in.	Exit Diameter, in.	Area Ratio	Maximum Model Impact Pressure, atm
a. Conventional Nozzles				
1.0	0.375	0.375	1.0	200
1.6	0.375	0.428	1.307	176
1.6	0.500	0.570	1.300	176
2.0	0.375	0.510	1.850	134
2.3	0.375	0.617	2.707	102
b. Internal Cold Shroud (ICS)				
2.0	0.919 (~0.372 core)	1.213	1.744	70

Table 2. Motion-Picture Log

Run No.	Camera No.	Camera Type	Film Type	Film Speed, fps	Shutter Speed, sec	Lens Focal Length, in.	F-Stop	Filter
1	1	Hycam	7242	400	1/6000	6	8	Split 2.0
	2	Locam	7242	400	1/1000	6	Automatic Exposure	N.D. 0.60
	3	Locam	7242	400	1/2000	6	22	N.D. 1.0
2	1	Hycam*	7242	-	-	6	8	Split 2.0
	2	Locam	7242	400	1/1000	6	Automatic Exposure	N.D. 0.90
	3	Locam	7242	400	1/2000	6	22	N.D. 1.0
3	1	Hycam	7242	400	1/6000	6	8	Split 2.0
	2	Locam	7242	400	1/1000	6	Automatic Exposure	N.D. 0.90
	3	Locam	7242	400	1/2000	6	22	N.D. 1.0
4,4A	1	Hycam	7242	100	1/200**	6	22	Split 2.0
	2	Locam	7242	100	1/260**	6	Automatic Exposure	N.D. 0.90
	3	Locam	7242	100	1/500**	6	22	N.D. 1.0
5	1	Hycam	7242	400	1/6000	6	22	Split 2.0
	2	Locam	7242	400	1/1000	6	Automatic Exposure	N.D. 0.90
	3	Locam	7242	400	1/2000	6	22	N.D. 1.0
6	1	Hycam	7242	400	1/6000	6	22	Split 2.0
	2	Locam	7242	400	1/1000	6	Automatic Exposure	-
	3	Locam	7242	400	1/2000	6	22	N.D. 1.20
7	1	Hycam	7242	400	1/6000	6	22	Split N.D. 2.0
	2	Locam	7242	400	1/1000	6	Automatic Exposure	-
	3	Locam	7242	400	1/2000	6	22	N.D. 1.20
8	1	Hycam	7242	400	1/6000	6	22	Split N.D. 2.0
	2	Locam	7242	400	1/1000	6	Automatic Exposure	N.D. 1.20
	3	Locam	7242	400	1/2000	6	22	-

*Camera did not run.
**Film underexposed.

53

Table 3. Run Log

Run No.: 1   Date: 2-19-75   Mach No.: 2.3   Nozzle Type: Conventional

Enthalpy: 2,309, Btu/lbm   Impact Pressure: 42.9 atm

Sting	Model No.	Model Position X, in.	Dwell Time, sec	Weight, gm		Mass Loss, gm	Photograph No.		Length, in.	
				Pretest	Posttest		Pretest	Posttest	Pretest	Posttest
1	Open	-	-	-	-	-	-	-	-	-
2	Pressure Model	0.10	Sweep	-	-	-	-	-	-	-
3	Calorimeter	0.10	Sweep	-	-	-	-	-	-	-
4	A11-S	0.10	5	49.209	39.350	9.859	1073	1443	2.000	1.378
5	A21-S	0.10	5	37.694	30.968	6.726	1052	1448	2.001	1.411
6	A31-S	0.10	5	76.978	54.866	22.112	1070	1444	2.000	1.291
7	A41-S	0.10	5	50.991	37.291	13.700	1063	1447	2.007	1.241

NOTE: Pressure and calorimeter models had nose radii (R_n) of 0.25 in. and seven and two data channels, respectively.

Calorimeter data channels 2, 3, and 4 were inoperative.

Table 3. Continued

Run No.: 2   Date: 2-20-75   Mach No.: 2.3   Nozzle Type: Conventional

Enthalpy: 2,416, Btu/lbm   Impact Pressure: 65.6, atm

Sting	Model No.	Model Position X, in.	Dwell Time, sec	Weight, gm		Mass Loss, gm	Photograph No.		Length, in.	
				Pretest	Posttest		Pretest	Posttest	Pretest	Posttest
1	Open	-	-	-	-	-	-	-	-	-
2	Pressure Model	0.10	Sweep	-	-	-	-	-	-	-
3	Calorimeter	0.10	Sweep	-	-	-	-	-	-	-
4	A13-C	0.10	3	43.563	35.197	8.366	1081	1577	1.999	1.413
5	A22-C	0.10	3	37.333	31.351	5.982	1053	1579	2.001	1.322
6	A43-C*	0.10	2	47.592	-	-	1065	-*	2.000	-
7	Open	-	-	-	-	-	-	-	-	-

*Model destroyed during test.

Table 3. Continued

Run No.: 3   Date: 2-26-75   Mach No.: 2.3   Nozzle Type: Conventional

Enthalpy: 2,242; Btu/lbm   Impact Pressure: 72.8, atm

Sting	Model No.	Model Position X, in.	Dwell Time, sec	Weight, gm		Mass Loss, gm	Photograph No.		Length, in.	
				Pretest	Posttest		Pretest	Posttest	Pretest	Posttest
1	Open	-	-	-	-	-	-	-	-	-
2	Pressure Model	0.10	Sweep	-	-	-	-	-	-	-
3	Calorimeter	0.10	Sweep	-	-	-	-	-	-	-
4	A15-C	0.10	2	47.110	36.262	10.838	1082	2099	1.999	1.355
5	A32-C	0.10	2	77.565	52.739	24.826	1069	2101	2.003	1.094
6	A44-C	0.10	2	52.150	33.574	18.576	1067	2102	2.001	0.974
7	8S-12-1	0.10	4	21.876	18.044	3.832	1865	2100	1.977	1.413

Table 3. Continued

Run No.: 4   Date: 3-28-75   Mach No.: 2.0   Nozzle Type: ICS

Enthalpy: 2,120, Btu/lbm   Impact Pressure: 50.5, atm

Sting	Model No.	Model Position X, in.	Dwell Time, sec	Weight, gm		Mass Loss, gm	Photograph No.		Length, in.	
				Pretest	Posttest		Pretest	Posttest	Pretest	Posttest
1	Open	-	-	-	-	-	-	-	-	-
2	Pressure Model	0.10	Sweep	-	-	-	-	-	-	-
3	Calorimeter	0.10	Sweep	-	-	-	-	-	-	-
4	Pressure Probe*	-	Traverse	-	-	-	-	-	-	-
5	Open	-	-	-	-	-	-	-	-	-
6	Open	-	-	-	-	-	-	-	-	-
7	Open	-	-	-	-	-	-	-	-	-

*Carbon tip pressure probe (R_n 0.25 in.) injected approximately 5 in. downstream of nozzle, then moved toward nozzle exit. Model failed before it reached 0.10-in. station.

Table 3. Continued

Run No.: 4A   Date: 3-28-75   Mach No.: 2.0   Nozzle Type: ICS

Enthalpy: 2,222, Btu/lbm   Impact Pressure: 72.3, atm

Sting	Model No.	Model Position X, in.	Dwell Time, sec	Weight, gm		Mass Loss, gm	Photograph No.		Length, in.	
				Pretest	Posttest		Pretest	Posttest	Pretest	Posttest
1	Open	-	-	-	-	-	-	-	-	-
2	Pressure Model	0.10	Sweep	-	-	-	-	-	-	-
3	Calorimeter	0.10	Sweep	-	-	-	-	-	-	-
4	Pressure Probe*	Traverse	-	-	-	-	-	-	-	-
5	Open	-	-	-	-	-	-	-	-	-
6	Open	-	-	-	-	-	-	-	-	-
7	Open	-	-	-	-	-	-	-	-	-

*Pressure probe (graphite) R_n 0.50 in. injected approximately 4 in. downstream of nozzle exit on centerline, then moved toward nozzle.

Table 3. Continued

Run No.: 5   Date: 4-2-75   Mach No.: 2.0   Nozzle Type: ICS

Enthalpy: 2,172, Btu/lbm   Impact Pressure, Varied, atm

Sting	Model No.	Model Position - X, in.	Dwell Time, sec	Weight, gm		Mass Loss, gm	Photograph No.		Length, in.	
				Pretest	Posttest		Pretest	Posttest	Pretest	Posttest
1	Open	-	-	-	-	-	-	-	-	-
2	Pressure Model	1.00	Sweep	-	-	-	-	-	-	-
3	Calorimeter	2.00	Sweep	-	-	-	-	-	-	-
4	A33-C	Traverse	10*	82.135	35.600	46.535	1068	2651	2.000	0.825
5	Open	-	-	-	-	-	-	-	-	-
6	A34-S	Traverse	10*	82.373	37.208	45.173	1454	2654	1.982	N.A. (Broke Up)
7	AT2-S	0.10	3	-	20.5	-	-	2656	2.003	1.775

*Note model injected 4.0 in. from nozzle exit, moved forward; however, model ablated the preset distance (0.5 in.) before it reached the 0.10-in. test position and was automatically ejected.

Table 3. Continued

Run No.: 6   Date: 4-4-75   Mach No.: 2.0   Nozzle Type: ICS

Enthalpy: *, Btu/lbm   Impact Pressure: *, atm

Sting	Model No.	Model Position X, in.	Dwell Time, sec	Weight, gm		Mass Loss, gm	Photograph No.		Length, in.	
				Pretest	Posttest		Pretest	Posttest	Pretest	Posttest
1	Open	-	-	-	-	-	-	-	-	-
2	Pressure Model	1.00	Sweep	-	-	-	-	-	-	-
3	Calorimeter	1.00	Sweep	-	-	-	-	-	-	-
4	A12-S	Traverse	2**	44.301	39.800	4.501	1074	2833	2.001	1.815
5	Open	-	-	-	-	-	-	-	-	-
6	C11-S	Traverse	4**	22.129	22.100	0.029	1866	2831	1.977	1.970
7	A45-C	0.10	2**	48.812	48.200	0.612	1066	2837	2.001	2.000

*Due to malfunction of model injection system, tunnel data were not reduced.

**Model A12-S injected 4.0 in. from nozzle exit, moved forward to the 0.10-in. test station. The injection system malfunctioned on Positions 6 and 7; models did not move forward.

Table 3. Continued

Run No.:7   Date: 4-7-75   Mach No.: 2.0   Nozzle Type: ICS

Enthalpy: 2,275, Btu/lbm   Impact Pressure: 78.1, atm

Sting	Model No.	Model Position X, in.	Dwell Time, sec	Weight, gm		Mass Loss, gm	Photograph No.		Length, in.	
				Pretest	Posttest		Pretest	Posttest	Pretest	Posttest
1	Open	-	-	-	-	-	-	-	-	-
2	Pressure Model	0.30	Sweep	-	-	-	-	-	-	-
3	Calorimeter	0.30	Sweep	-	-	-	-	-	-	-
4	A42-S	Traverse	4*	52.371	31.000	21.371	1064	2841 2838	1.993	Model broke up
5	Open	-	-	-	-	-	-	-.	-	-
6	C11-C	Traverse	4	22.251	19.500	2.751	1863	2840	2.002	1.630
7	Open	-	-	-	-	-	-	-	-	-

*Models injected 4.0 in. from nozzle exit, moved forward to test station.

Table 3. Concluded

Run No.: 8 | Date: 4-9-75 | Mach No.: 2.0 | Nozzle Type: Conventional

Enthalpy: 2,302, Btu/lbm | Impact Pressure: 92.8, atm

Sting	Model No.	Model Position X, in.	Dwell Time, sec	Weight, gm		Mass Loss, gm	Photograph No.		Length, in.	
				Pretest	Posttest		Pretest	Posttest	Pretest	Posttest
1	Open	-	-	-	-	-	-	-	-	-
2	Pressure Model	0.10*	Sweep	-	-	-	-	-	-	-
3	Calorimeter	0.10	Sweep	-	-	-	-	-	-	-
4	A14-C	0.10	1.5	49.107	41.900	7.207	1080	2844	2.000	1.520
5	A23-C	0.10	1.5	37.560	32.000	5.560	1054	2848	2.001	1.600
6	A16-S	0.10	1.5	54.923	47.000	7.923	1451	2850	2.001	1.625
7	8S-12-2	0.10	2.0	22.082	19.200	2.882	1864	2853	2.005	1.530

*Model injection system operated at a fixed axial position. Models injected 0.10 in. downstream of nozzle exit.

Table 4. Model Pyrometer Data

Run No.	Model No.	Maximum Brightness Temperature, °F		Remarks
		Pyrometer No. 316	Pyrometer No. 317	
1	A11-S	4302	4352	
	A21-S	3857	3841	
	A31-S	3556	3459	
	A41-S	3862	3657	
2	A13-C	3933	3436	
	A22-C	4193	4024	
	A43-C	-	-	Model destroyed
3	A15-C			Models ejected before they reached 0.10-in. test station
	A32-C			
	A44-C			
	8S-12-1			
5	A33-C			Model never reached test station
	A34-S			Model never reached test station
	AT-2S	4124	5199	
6	A12-S			Model injection system
	C11-S			malfunctioned
	A45-C			Data not valid
7	A42-S*			*Model ablation rate such that
	C11-C	3180	3631	ablating surface never reached 0.10-in. station
8	A14-C	3784	4660	
	A23-C	3736	4524	
	A16-S	4044	4954	
	8S-12-2	4884	5078+*	*Off-scale

NOMENCLATURE

C   Cone–cone

$d*$ Throat diameter

H_O Enthalpy reservoir conditions from energy balance, Btu/lbm

h_W Enthalpy at wall conditions, Btu/lbm

M   Mach number

p   Local pressure, atm

p_O Reservoir pressure, psia, atm

p_O' Impact pressure, atm

$p_{O_{C_L}}'$ Impact pressure on nozzle centerline, atm

p_{sp} Model stagnation point pressure, atm

$\dot{q}_{cw}$ Cold wall heat-transfer rate, Btu/ft^2-sec

$\dot{q}_{hw}$ Hot wall heat-transfer rate, Btu/ft^2-sec

R_n Nose radius

S   Sphere-cone, or distance along cone surface from stagnation point, in.

X   Axial position of model from nozzle exit plane, in., or distance downstream of tangent point on model, in.

α Polar angle, deg

γ Ratio of specific heats or reentry angle, deg

θ Cone half-angle, deg (sphere-cone models)

θ_1, θ_2 Cone half-angle, deg (cone-cone models)

ϕ Hemisphere latitude angle, deg